Hindawi
Modelling and Simulation in Engineering
Volume 2018, Article ID 1932813, 20 pages
https://doi.org/10.1155/2018/1932813

Research Article

Numerical Study on Diffusion of Chloride and Induced Rebar Corrosion by Two-Dimensional Multiscale Approach

Xi Tu[1,2], **Jin Di**[1,2], **Cunjun Pang**[1,2] **and Xiaoqing Xu**[1,2]

[1]*Key Laboratory of New Technology for Construction of Cities in Mountain Area (Chongqing University), Ministry of Education, Chongqing, China*
[2]*College of Civil Engineering, Chongqing University, Chongqing, China*

Correspondence should be addressed to Xi Tu; tuxi@cqu.edu.cn

Received 15 November 2018; Accepted 12 December 2018; Published 31 December 2018

Guest Editor: Qing-feng Liu

Modeling approach for mesoscopic model of concrete depicting mass transportation and physicochemical reaction is important since there is growing demand for accuracy and computational efficiency of numerical simulation. Mesoscopic numerical simulation considering binder, aggregate, and interfacial transition zone (ITZ) generally produces huge number of DOFs, which is inapplicable for full structure. In this paper, a two-dimensional multiscale approach describing three-phase structure of concrete was discussed numerically. An effective approach generating random aggregate in polygon based on checking centroid distance and intersection of line segment was introduced. Moreover, ITZ elements were built by parallel expanding the edge of aggregates on inner side. By combining mesoscopic model including full-graded aggregate and macroscopic model, cases related to diffusivity and width of ITZ, volume fraction, and grade of aggregate were studied regarding the consideration of multiscale compensation. Result clearly showed that larger analysis model in multiscale model expanded the diffusion space of chloride ion and decreased chloride content in front of rebar. Finally, this paper addressed some noteworthy conclusions about the chloride distribution and rebar corrosion regarding the configuration of rebar diameter, concrete cover, and exposure period.

1. Introduction

Corrosion of rebar induced by chloride ion could significantly deteriorate the serviceability of concrete structures [1]. The protective film of rebar was depassivated by chloride ion penetrated from surface of concrete and thus corrosion of rebar initiates once the chloride content on surface of rebar reaches a certain thresholding value, defined as critical chloride content. Afterwards, corrosion of rebar keeps propagating and induces further cracking and spalling due to expansion of rust. Therefore, it is important to accurately assess the diffusion process of chloride ion within concrete, which is meaningful for further evaluation of durability of reinforced concrete structures.

In the view of mesoscopic numerical simulation, concrete was recognized as the heterogeneous composite of three phases, including cement paste, aggregate, and interfacial transition zone (ITZ) [2]. ITZ was identified as a fine cement paste zone enclosing aggregate and rebar, providing higher water-to-cement ratio, higher porosity, and lower cement content compared with normal bulk cement paste regions. Thus ITZ was generally considered as an individual phase [3–5]. Though the porosity of ITZ decreases with increase of distance from aggregate surface [6], ITZ was simplified as a homogenous thin layer in most studies. Significant influence on the overall behavior of concrete attributes to ITZ due to its fraction of the total paste volume, such as diffusivity and strength [4, 6–8].

In the view of mesoscopic numerical simulation, due to large amount of nodes and elements, an optimized approach was that three-phase composite of concrete was simplified into two-phase composite including cement paste and homogenized equivalent aggregate [4, 7, 9–13]. Diffusivity of ITZ was transferred by means of deriving the analytical solution of general effective chloride diffusivity, which means modeling of ITZ is unnecessary.

Generally, modeling and analysis for cement-based material were categorized in microscopic scale, mesoscopic scale,

and macroscopic scale [14, 15]. Recently a number of theory research and modeling efforts have been devoted to studying multiscale modeling. Multiscale modeling was usually defined as the integrated numerical process of transferring mechanical and chemical response between lower scale and higher scale [16, 17]. A significant advantage of multiscale modeling is optimizing computing loading and enhancing the precision. According to available literature, researchers generally focused on the transferring process of material response between scales.

As the major purpose of multiscale modeling to reduce calculation loading, heterogeneous model was always modeled for transferring damage and mass transportation of critical regions from the macroscale to the mesoscale which provided coupling of subdomains [18]. Balance of accuracy and efficiency is the major consideration of multiscale modeling for numerical simulation. By means of macroscopic model substituting for a part of mesoscopic model, multiscale modeling is able to provide relatively smaller size of mesoscopic model and generate the same filling rate of aggregate and less amount of aggregate, which is no doubt beneficial for raising success rate of meshing [19].

For mesoscopic structure of concrete, both of size and shape of aggregates are generated as given design. Regarding two-dimensional space, general process was divided into two steps, including modeling of geometric model and meshing. Angular aggregate was generated based on inscribed convex polygon within elongated ellipse [20]. Wang et al. proposed a procedure for generating random aggregate structures for angular aggregates by means of Monte Carlo sampling, which was compatible for concave polygon [21]. An inevitable algorithm was intersection check of convex polygons, which was achieved by detecting space independence of two polygons [22, 23]. In terms of meshing, mortar plus smaller aggregates embedding coarse aggregate was discretized into finite elements by free meshing [20, 24] or uniform background grid [25–27].

Another major factor for durability of reinforced concrete structures is corrosion of steel rebar. Researchers devoted efforts on laboratorial research by means of natural experiments [28–32] and accelerated experiments [33–38] about the process of chloride diffusion and corrosion. On the other hand, some types of simplified approximate law for corrosion were introduced. Biondini introduced a reasonable linear damage model for corrosion of rebar under aggressive agent, which evaluates corrosion rate according to the real-time chloride content surrounding rebar [39–42]. Despite the complex principle of corrosion, based on the natural damage mode of corrosion, this linear damage model is able to provide acceptable description of damage process.

This paper discussed two important aspects regarding multiscale modeling for numerical simulation of chloride ion diffusing within concrete. Firstly, a comprehensive modeling approach for concrete considering both multiscale modeling including interfacial transition layer (ITL) and three-phase mesoscale structure including ITZ. Secondly, by means of the multiscale numerical simulation tool, the influence of ITZ on diffusion of chloride ion within concrete in mesoscale was studied in detail, where ITZ was modeled as an individual phase in FE model for chloride diffusion in concrete. Besides, the corrosion of rebar in straight edge of concrete induced by diffusion of chloride ion was also calculated to study the time evolution of corrosion process.

2. Multiscale Modeling and Discussion

2.1. Multiscale Modeling Theory. In mesoscopic numerical simulation for chloride diffusion, usually 100~200 mm size of specimen in square or rectangle was considered. Within this typical size of analysis space, enough number of aggregates with various sizes were included for in-depth study. Within limited analysis space, chloride ion would able to penetrate and saturate the whole space within the assessing period, indicating the whole space was inadequate for further simulation. However, it would be impossible to increasing the size of analysis space due to two reasons. First, several times of original size of analysis space will generate much more nodes and elements, especially for three-dimensional problem. Second, to control computing loading, changing the grading curve and ignoring fine aggregate will cause inaccuracy of numerical simulation.

In this paper, a scheme of multiscale modeling was introduced in terms of balancing amount of nodes and elements and calculation accuracy (Figure 1). In the view of multiscale modeling, based on original mesoscopic model including multiphase components which was defined as core part, a macroscopic compensation model, which was defined as compensation part, was modeled. The aim of introducing compensation part was creating addition space to absorb the chloride within core part and adjusting the distribution of chloride content within core part, which means redistribution of chloride in larger space.

Due to different definition of nodal chloride content and diffusion coefficient in mesoscopic model and macroscopic model, the two types of models cannot be directly combined and analyzed simultaneously. In this paper, interfacial transition layer (ITL) was introduced to connect both models at the interface which consists of a group of nodes and elements, shown in Figure 1. ITL was designed as a banded shape transition zone allowing chloride ion diffusing from core part into compensation part. Within each time step, core part and compensation part were analyzed sequentially and the chloride content at interface of the two parts was transferred based on the function of ITL.

It is worth noting that the most important precondition is the mechanism of ITL for transporting the chloride ion, which generates equivalent diffusion and distribution of chloride within the model on the same scale. ITL could be composed by a row of common nodes occupied by both mesoscopic model and macroscopic model, as well as an amount of elements with certain thickness stuck by both models.

The process of transferring chloride ion within ITL in one-dimension was illustrated in Figure 2. For initial state, analysis space of three phases including core part, compensation part, and ITL was modeled, respectively. Boundary condition was set at surface of concrete, which was the top of core part shown in Figure 2.

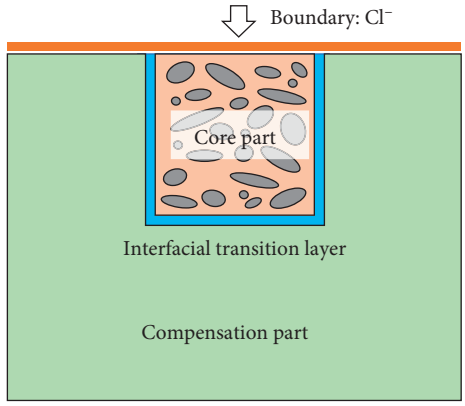

Figure 1: Two-dimensional multiscale model with core part and compensation part for simulating chloride diffusion within concrete.

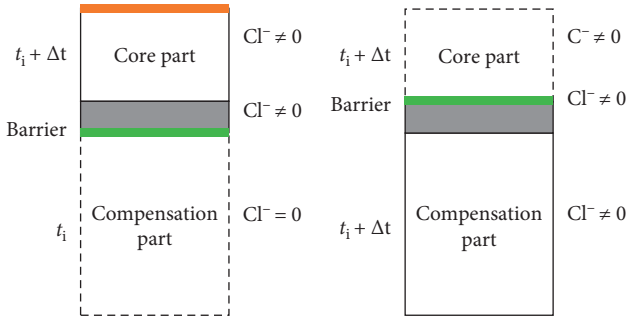

Figure 2: The two stages of chloride diffusion at the interfacial transition layer connecting macroscopic and mesoscopic model. (a) First stage. (b) Second stage.

This mixed model behaved in sequential multiscale process. For the mixed case that core part is in mesoscale and compensation part in macroscale, equivalent chloride content in ITL will be calculated and transferred. Definitions of chloride content in both parts were different. Chloride content in macroscopic model was measured in concrete, and the value in mesoscopic model was measured in cement. Therefore, a necessary procedure was included that the value of chloride content in ITL should be calculated for each stage. Simulation of chloride diffusion within mixed model was divided into two stages of diffusion and two steps of conversion.

(1) The first stage of diffusion: core part and ITL were connected as common interface while ITL and compensation part were disconnected. With one time step, chloride ion penetrated into core part from boundary condition. During current stage, diffusion of chloride ion restrained within core part and ITL. The chloride content of core part and ITL rose up from previous content while compensation part kept unchanged.

Find out all of the elements with the centroid located within the elements from compensation model.

Calculate the weighted mean content of all these elements in core model. This content is the represented content for the element in compensation model.

(2) Conversion from mesoscale to macroscale within ITL: the simulated result in region in core part covered by ITL was converted from mesoscale to macroscale within this step. For the instance of center bottom of concrete boundary, compensation part was modeled as simply one-dimensional model. Within core part, elements with their centroid included in interfacial transfer layer were identified (the region enclosed by red dashed line in Figure 3). Weighted mean value of chloride content of these involved elements was calculated for the nodal value of ITL in macroscale.

(3) The second stage of diffusion: a new barrier was inserted at common border of core part and ITL which was equal to cut down the connection of these parts. The existing barrier at common border of compensation part and ITL was removed. During this stage, chloride redistributes within the region including ITL and compensation part.

(4) Conversion from macroscale to mesoscale within ITL: as the inverse process of the 2nd step, the nodal content of mesoscopic core part was interpolated from macroscopic compensation part in the form of regular rectangle element. As was illustrated in Figure 4, the outer rectangle represents the uniform quadrilateral model in compensation part and the target node denotes the node included within core part. Four nodes of the quadrilateral were numbered in counterclockwise.

2.2. Analytical Study for Finite Space with Exposed and Time-Dependent Boundary. In following section, this paper discussed about the feasibility of multiscale model in analytical approach. Due to the sectional design of rebar in concrete member, some research studies on chloride diffusion were transformed within two-dimensional space equivalently. For the case on center of bottom of concrete section, concrete and outer atmosphere were divided into two infinite half-space into which the boundary plane divides the three-dimensional space. Regarding numerical simulation, for the same configuration of boundary condition and diffusivity of concrete, all points in concrete at the same depth from the boundary behave in the same characteristics of diffusion. In simplification, the chloride diffusion in three-dimensional and two-dimensional space was equivalent to one-dimensional one. Therefore, the problem was simplified to one-dimensional macroscopic model, and the analytical solution for finite space with both exposed and sealing boundary was discussed. Usually diffusion of chloride within solution was expressed by linear Fick's second law:

$$\frac{\partial C}{\partial t} = D \cdot \nabla^2 C, \tag{1}$$

where D is the diffusion coefficient of concrete. C denotes the chloride content. Considering the boundary condition of $C(0,t) = C_s$ and $C(\infty,t) = C_0$. As was widely known, according to Laplace transform, the analytical solution of above partially derivative equation was

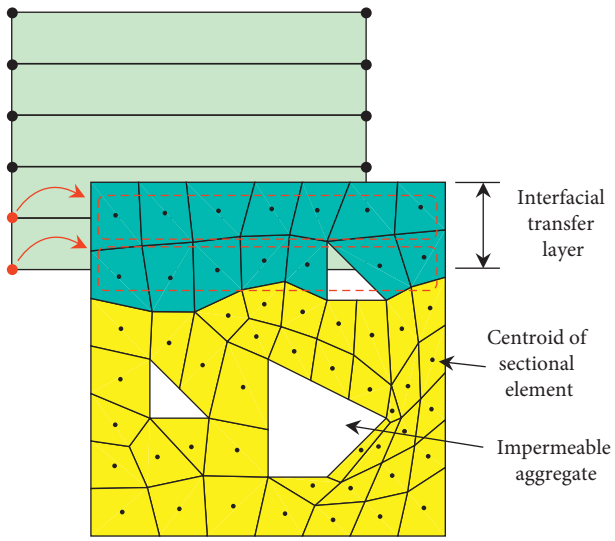

Figure 3: First step of conversion: calculation of nodal chloride content of compensation part from involved elements in core part (red dashed: coverage of nodes in compensation part; blue: involved elements in core part; yellow: uninvolved elements).

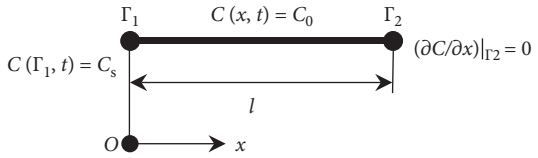

Figure 4: Analysis model for analytical deduction.

$$C(x,t) = C_0 + (C_s - C_0)\left[1 - \operatorname{erf}\left(\frac{x}{2\sqrt{Dt}}\right)\right], \quad (2)$$

where erf is Gauss error function. The limitation of the above solution is the premise of infinite space for boundary condition, which is suitable for concrete members with large thickness compared with thickness of concrete cover, but inaccurate for typical beams and slabs. For finite space, three-dimensional analytical solution by means of separation of variables was discussed and deduced by Li et al. [43]. For one-dimensional space, assuming the total length of diffusion space is l. x axis is the longitudinal direction of the one-dimensional model. Initial condition for diffusion space, $C(x,0) = C_0$ and boundary condition, exposed boundary $C(\Gamma_1, t) = C_s$, and sealing boundary $\partial C/\partial x|_{\Gamma_2} = 0$ were all considered. The schematic illustration is shown in Figure 4.

The simplified function of chloride content including the variables of time and depth in one-dimensional space according to Li's solution was expressed as follows:

$$C = C_s + (C_0 - C_s)\sum_{n=1}^{\infty}\frac{4}{(2n-1)\pi}\sin\left(\frac{2n-1}{2l}\pi x\right)e^{-D(((2n-1)/2l)\pi)^2 t}. \quad (3)$$

If zero chloride content for initial condition, $C_0 = 0$, was considered, equation (3) was simplified as given below:

$$C = C_s\left[1 - \sum_{n=1}^{\infty}\frac{4}{(2n-1)\pi}\sin\left(\frac{2n-1}{2l}\pi x\right)e^{-D(((2n-1)/2l)\pi)^2 t}\right]. \quad (4)$$

The aim of following section was to deduce the expression of analytical solution of chloride content with both exposed boundary and time-dependent boundary according to Li's deduction process and prove that the development in core model with predefined time-dependent boundary condition is same as the part in full model. For the consideration of compensation for chloride diffusion, a part of the full model was extracted and called as *Core Model*. The schematic illustration of core model was shown in Figure 5. The length of core model was l_1 while assuming the length of full model was l_2 ($l_2 > l_1$).

Being different with the precondition of Li's solution [43], the boundary condition Γ_2 of core model was modified into the function of time-dependent boundary Γ_2' strictly defined by equation (4) set at l_1, expressed in equation (5). The other parameters and definition were the same as before. For simplification, zero chloride content for initial condition, $C_0 = 0$, was considered.

$$C(t)|_{\Gamma_2} = C_s\left[1 - \sum_{n=1}^{\infty}\frac{4}{(2n-1)\pi}\sin\left(\frac{2n-1}{2l_2}\pi l_1\right)e^{-D\left((2n-1)/2l_2\pi\right)^2 t}\right]. \quad (5)$$

Considering a temporary variable V,

$$V = C - C_s. \quad (6)$$

Apart from initial condition and boundary condition, the time-dependent boundary Γ_2' was expressed as

$$V|_{x=l_1} = -C_s\sum_{n=1}^{\infty}\frac{4}{(2n-1)\pi}\sin\left(\frac{2n-1}{2l_2}\pi l_1\right)e^{-D\left((2n-1)/2l_2\pi\right)^2 t}. \quad (7)$$

By means of separation of variables, V was expressed as

$$V(x,t) = X(x)\cdot T(t). \quad (8)$$

By introducing boundary condition of exposed surface Γ_1, the general solution of X was simplified as

$$X(x) = B\sin(\alpha x). \quad (9)$$

For time-dependent boundary Γ_2', by combining equations (7) and (9), we obtained the expression of α:

$$\alpha_n = \frac{2n-1}{2l_2}\pi, \quad (n = 1, 2, \ldots). \quad (10)$$

Thus, particular solution of X was

$$X_n(x) = k_n\sin\left(\frac{2n-1}{2l_2}\pi x\right). \quad (11)$$

The particular solution of T was solved as

$$T_n = -d_n e^{-D\alpha_n^2 t}. \quad (12)$$

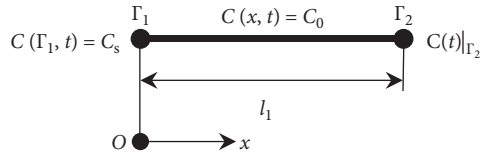

Figure 5: Illustration of core model for diffusion with compensation.

Thus, general solution of V was

$$V_n = e_n \sin\left(\frac{2n-1}{2l_2}\pi x\right) e^{-D\alpha_n^2 t}. \tag{13}$$

where e_n was the nth order of unknown expression and $e_n = k_n \cdot d_n$. Considering initial condition ($t = 0$), we obtained the following from equation (13):

$$\sum_{n=1}^{\infty} e_n \sin\left(\frac{2n-1}{2l_2}\pi x\right) = -C_s. \tag{14}$$

Due to orthogonality of the following function series,

$$\int_0^l \sin(\alpha_m x)\sin(\alpha_n x)dx = \begin{cases} 0, & m \neq n, \\ l/2, & m = n, \end{cases} \tag{15}$$

Combining equations (14) and (15), we obtained:

$$e_n = -\frac{4C_s}{(2n-1)\pi}. \tag{16}$$

By combining equations (6), (13), and (16), finally we obtained:

$$C = C_s\left[1 - \sum_{n=1}^{\infty} \frac{4}{(2n-1)\pi} \sin\left(\frac{2n-1}{2l_2}\pi x\right) e^{-D\left(\left((2n-1)/2l_2\pi\right)\right)^2 t}\right], \quad (x \in [0,\ l_1]). \tag{17}$$

Therefore, even considering the time-dependent boundary, the development of diffusion within core model was exactly the same as the original model, which proved the feasibility of compensation for chloride diffusion.

3. Mesoscopic Modeling Approach

3.1. Generation of Two-Dimensional Random Aggregate. In two-dimensional space, the major consideration of generating mesoscopic model is requirement of both grading of aggregates and its volume fraction in concrete. Generally, the mesoscopic structure of aggregate is randomly generated by dispersing particles in given shape and size in a limited square or rectangle space. This process was fulfilled by two essential steps, including constructing qualified aggregate and dispersing the aggregate. An applicable approach introduced in this paper was depicted as follows.

(1) Construction of aggregate in given shape and size regarding grading of concrete: the convex polygon of an applicable aggregate is connected along the points on the curve of a randomly generated ellipse, the area of which meets the requirement of design particle size. Then, the preliminary inscribed polygon is enlarged to match the same area of designed ellipse.

Two additional points to guarantee reasonable shape of aggregate should be noted. In practical concrete engineering, elongated aggregate (with dimension ratio over 2 : 1) should be avoided considering its poor structural performance. Thus, in aggregate generation program, all vertices of polygon are well distributed on ellipse in terms of the included angle defined by the connecting line of vertices of polygon and its centroid (Figures 6(a) and 6(b)). Another measurement is controlling the area occupancy of polygon within the design ellipse (Figures 6(c) and 6(d)). Detailed values for minimum included angle and minimum area occupancy are designed by domestic specification for aggregates.

(2) Dispersing aggregate by judgement of overlapping of aggregates: within two-dimensional space, for one newly dispersed aggregate, checking its involvement within given rectangle analysis region and overlapping with all existing aggregates are required. The first condition can be met by checking whether the maximum and minimum coordinates of polygon are covered by the rectangle. The detailed judgement for overlapping of convex polygon was described as follows. Terms quoted are shown in Figure 7.

(i) For each pair of aggregates, judge whether sum of outer radius $(R_0 + R_0')$ is larger than distance of centroids (d_{agg}). Here, outer radius is defined as the maximum radical distance from any vertex to centroid. If no $((R_0 + R_0') \leq d_{agg})$, there is no overlapping of aggregate and the newly dispersed aggregate is accepted. If yes $((R_0 + R_0') \geq d_{agg})$, possible overlapping cannot be avoided and continue to next step for further check.

(ii) Judge whether sum of inner radius $(R_i + R_i')$ is smaller than distance of centroids (d_{agg}). Here, inner radius is defined as the minimum radical distance from any side to centroid. If no $((R_i + R_i') > d_{agg})$, solid overlapping appears and a redispersion of new aggregate is required. If equal $((R_i + R_i') = d_{agg})$, a rare case representing parallel sides of aggregates is inappropriate which is also unaccepted. If yes $((R_i + R_i') < d_{agg})$, intersected sides cannot be avoided continue to next step for further check.

(iii) Judge whether the vertices of polygon representing aggregate are inclusion of the existing aggregate (Figure 8). If yes, overlapping is proved and a redispersion of new aggregate is required. If no, a complicated case of overlapping that intersection polygons without any vertex located within each polygon still cannot be assured and continue to next step.

(iv) The last step is judging whether there are any shared nodes of background meshing grid for both polygons (Figure 9). If yes, overlapping is proved and a redispersion of new aggregate is

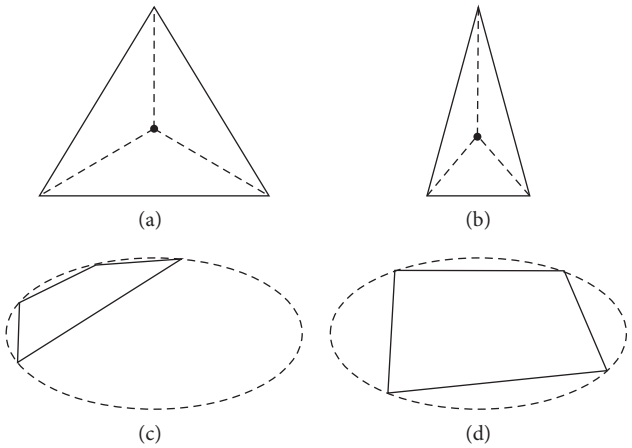

Figure 6: Generating polygon of aggregate based on ellipse. (a) Acceptable aggregate. (b) Elongated aggregate. (c) Low area proportion. (d) Fair area proportion.

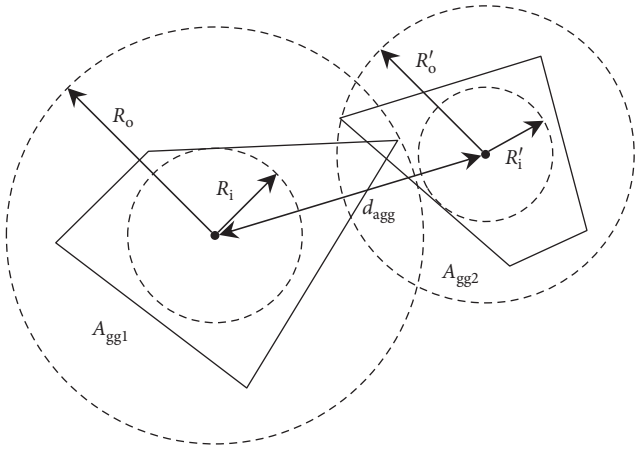

Figure 7: Inner radius, outer radius, and distance of centroids of two intersected aggregates.

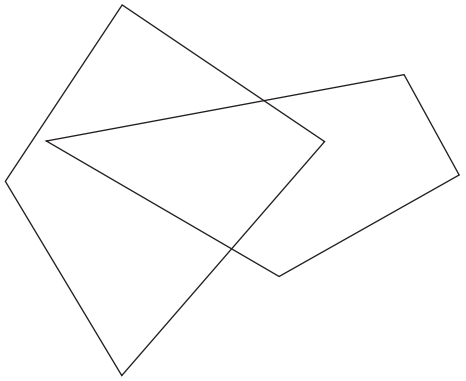

Figure 8: Inclusion of vertices owned by dispersed aggregate in existing aggregate.

required. If no, the newly dispersed aggregate is accepted.

The above process was illustrated in Figure 10. Two typical models with elongated aggregate are shown in Figure 11.

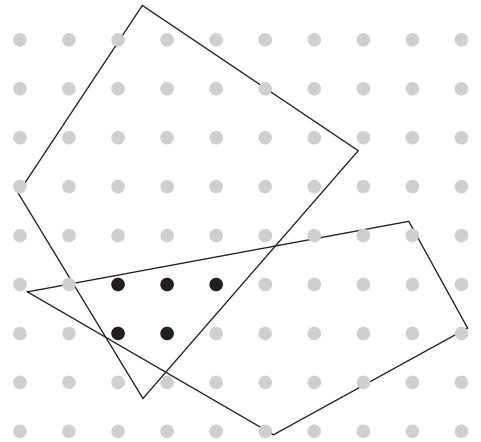

Figure 9: Shared nodes of background meshing grid for both polygons.

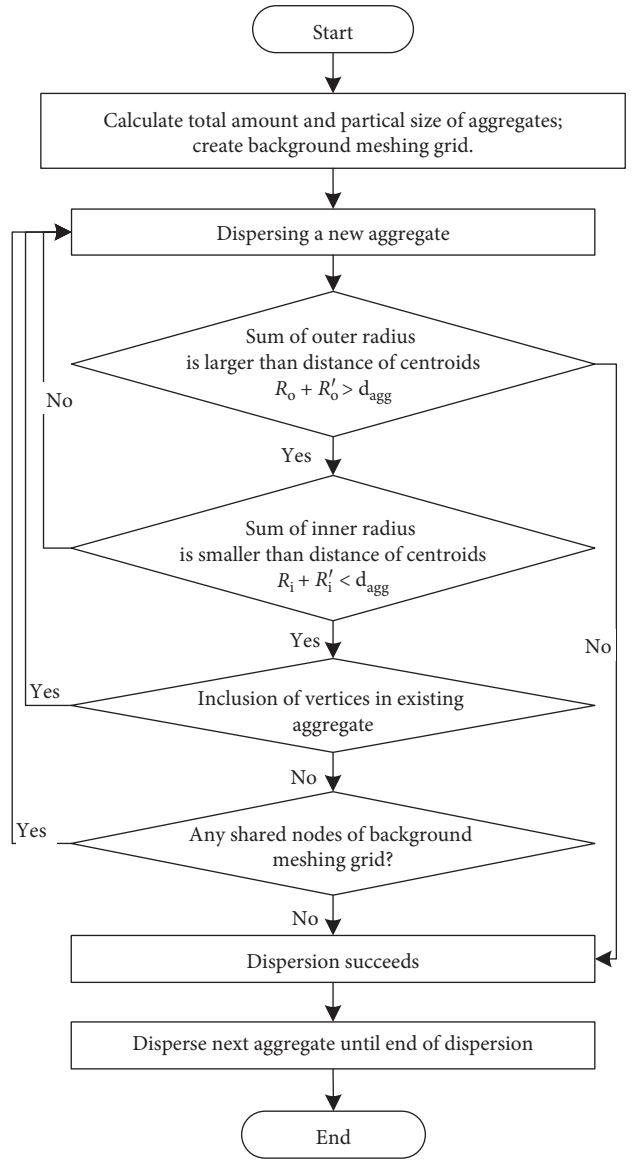

Figure 10: Process of generating random polygonal aggregates.

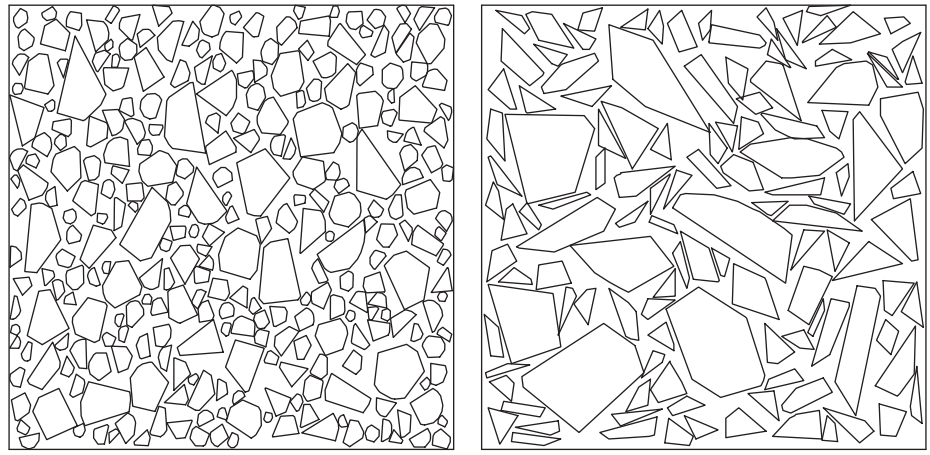

(a) (b)

Figure 11: Generated aggregates with limitation on dimension ratio. (a) Allowable dimension ratio up to 2 : 1. (b) Allowable dimension ratio up to 5 : 1.

Additional process for modeling is meshing the geometry space including significantly irregular distribution of aggregate. Conventional commercial software was adopted for meshing process. However, low success rate of meshing in refined quadrilateral element cannot be avoided for most commercial software due to the complex model. Thus, an optimized way adopted in this paper was meshing the space in triangle element and subdividing one triangle into four small quadrilaterals, which was proved as high meshing success rate and high efficiency.

3.2. Modeling of ITZ Based on Meshed Space. Modeling approach for ITZ was determined by the mechanism of simulating chloride diffusion within ITZ. ITZ was recognized as an indeterminate zone around aggregates and bulk, in linearly decreasing porosity with increase of distance from aggregate surface. Existing approaches describe ITZ as an individual layer or compensation on equivalent diffusivity of aggregate [44–46]. In terms of aggregates in random polygon, the way of building actual elements of ITZ was adopted in this paper. Thus, more DOFs were introduced, which significantly increased time consumption of assembling global diffusion matrix and solving it.

Since ITZ was identified as the individual phase surround aggregate, additional uniform width of elements adhering on the edge of aggregates might induce unnecessary overlapping of ITZ elements in some cases that the pair of aggregate was too close to each other. In order to avoid the above circumstance, ITZ elements were assigned on the inner side of edge of aggregate instead of outer side. According to minor area proportion of ITZ, it was acceptable slightly decreasing the size of aggregate. There are totally three steps for this process.

(i) For the first step, for any aggregate, the lines on its edge were parallel offset inside by the designed width, h, shown as the dashed line in Figure 12(a).

(ii) For the second step, all intersection of the offset lines were found, the total number of which were equal to vertices of aggregate, shown as the black point in Figure 12(b). Additionally, a special subroutine called "func_L2L" was developed to identify the relationship of a pair of line segments. Its output result provided whether the two line segments intersect and the coordinate of their intersection.

(iii) For the third step, combining the previous available nodes of aggregate and newly generated nodes (intersection), a group of quadrilateral elements was built in counterclockwise order, which represented ITZ. Their physical properties were set individually being different from existing cement paste.

The above entire process of modeling FE model of concrete involving ITZ is shown in Figure 13.

4. Basis of Assessing Approach

4.1. Diffusion Model of Chloride. Transportation of chloride ion in porous medium such as cementitious materials is mainly a diffusive phenomenon due to concentration gradients [47]. The diffusion of chloride ion within concrete components was admitted as a complex process, which was influenced by many factors including water/cement ratio, porosity of cement, additive, aggregate, temperature, humidity, environmental chloride content, binding effect of binder, and hydration of cement. The above process could be simulated by numerical approach based on available environmental attacking condition and material properties. Fick's second law was widely adopted as the expression of principle differential equation [48]:

$$\omega_e \frac{\partial C_f}{\partial t} = \frac{\partial}{\partial x} D_e \omega_e \frac{\partial C_f}{\partial x} - \frac{\partial C_b}{\partial t},$$
$$C_t = C_b + C_f \cdot \omega_e, \tag{18}$$

where C_f is the free chloride content (in kg/m^3 of solution); C_b is the bound chloride content (in kg/m^3 of concrete); C_t is the total chloride content (in kg/m^3 of concrete); D_e is the

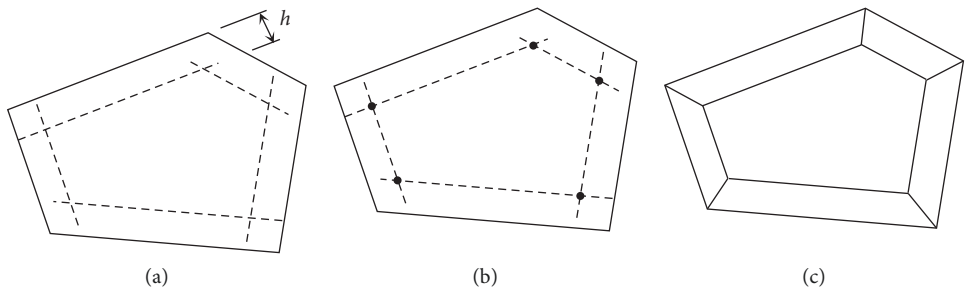

Figure 12: Process of generating new elements and nodes for ITZ. (a) Step 1: offset outline with ITZ width, h. (b) Step 2: find intersection (nodes) of outline. (c) Step 3: form elements of ITZ.

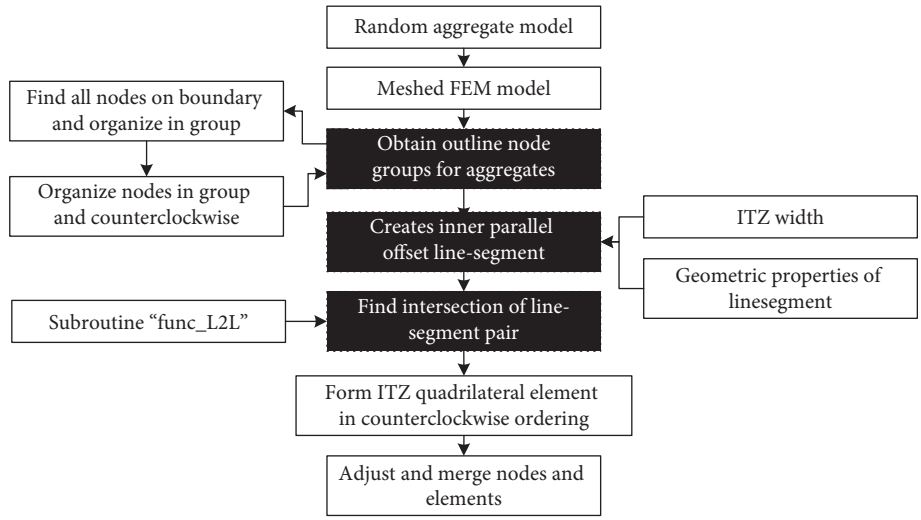

Figure 13: Flow chart for modeling of ITZ based on meshed FEM model.

effective diffusivity; and ω_e is the evaporable water content (in volume percentage of concrete). Considering complexity of cross sections of bridge pier, appropriate preliminary division and meshing grid are processed by means of some meshing tools or commercial FE software. Experimental data indicated that due to cement hydration and chloride content, the chloride diffusion coefficient is strongly dependent on the exposure period of concrete [49].

4.2. Corrosion Model of Rebar. Corrosion of rebar initiates in the form of galvanic reaction between ferrous and oxygen accelerated by the presence of active free chloride ion once the protection of high pH (>12.5) hydration products was depassivated. Corrosion continues with the cycle of electric current between cathode and anode, which was influenced by high chloride concentration at the level of the rebar, environmental temperature, electrical resistivity of concrete, and hydration of cement. The corrosion model regressed by Liu and Weyers [34] based on experimental data included the influence of chloride content, temperature, concrete cover resistance, and time of cement hydration, which was expressed as

$$\ln\left(1.08 i_{\text{corr}}\right) = 8.37 + 0.618 \cdot \ln\left(1.69\text{Cl}\right) - \frac{3034}{T} - 0.000105 R_c + 2.32 t^{-0.215}, \quad (19)$$

where i_{corr} is corrosion current intensity (μA/cm^2); Cl is chloride content (kg/m^3), which was obtained from numerical simulation result of chloride diffusion; T is temperature at the depth of steel surface (in degree Kelvin); R_c is the resistance of the cover concrete (ohms); and t is corrosion time duration (years). With the data chloride content obtained by numerical simulation and the other parameters assumed previously, the real-time corrosion current rate at each time step of numerical simulation was calculated by equation (19). Thus, the corrosion depth on surface of rebar was calculated as [50]

$$D_{t+\Delta t} = D_t - 0.023 \cdot i_{\text{corr}} \Delta t, \quad (20)$$

where D_t is remaining rebar diameter (mm) at t years, here 20 mm adopted; $D_{t+\Delta t}$ is reduced rebar diameter (mm) at $t + \Delta t$ years; and $\Delta D|_{\Delta t}$ is reduction of rebar diameter (mm) for the period of propagation for the duration time of Δt years.

5. Numerical Simulation for Diffusion of Chloride Including Compensation

5.1. Influence of ITZ Properties regarding Compensation. Considering that characteristics of ITZ significantly influence diffusion chloride within concrete, critical properties of

ITZ were detailed studied in this section, including diffusivity and width of ITZ, aggregate volume fraction, and grade of aggregate. Furthermore, chloride content on surface of rebar was also researched regarding presence of ITZ.

Another major consideration of this paper was the effect of compensation in multiscale modeling. A 100×100 mm two-dimensional square space was modeled for mesoscopic core part, and another 100×200 mm rectangle space was modeled for macroscopic compensation part (Figure 14). Width of ITL was set at 10 mm, which means 10% area of core part and 5% area of compensation part were overlapped. On the other hand, for the case without compensation, macroscopic compensation part was deleted and chloride ion can only diffuse within smaller mesoscopic core part.

For the other parameters, transportation mechanism of chloride ion between both parts was described in previous section of this paper. For all simplified cases studied in this section, the analytical apparent surface chloride content of 0.71 (%w_c) and apparent concrete diffusivity of 1.84×10^{-12} m^2/s were adopted for macroscopic model, which were regressed based on Zhao's data [51]. Meanwhile, the aggregate was considered as impermeable and corresponding modeling of FEM was ignored. Boundary condition and diffusivity of cement paste were calculated by these results. Regarding generating random aggregate of mesoscopic model, Fuller's curve was adopted as the grading of aggregate. Both types of cases with compensation and without compensation were studied.

Significant random distribution of aggregate was the major factor for uncertainty of chloride diffusion. Thus, totally, 100 specimens of aggregate model for each case were generated and analyzed considering reasonable accurate and acceptable time consumption. After all specimens were analyzed, mean results of these cases were calculated for further comparison.

5.1.1. Diffusivity of ITZ. Firstly, diffusivity of ITZ was studied, which was represented by the ratio of D_{ITZ}/D_{CP}. Here, D_{ITZ} and D_{CP} denoted the diffusivity in ITZ and cement paste, respectively. As was discussed by Zheng et al. [4], D_{ITZ}/D_{CP} would vary within 1~5 considering different configuration of w/c, aggregate size, hydration time, and aggregate fraction theoretically, which were discussed by means of the approach introduced in this paper. 50 μm of ITZ width was modeled by expanding the edge of aggregate and rebar. Maximum aggregate size in 20 mm was considered.

Figure 15 showed typical distribution of chloride content regarding different diffusivity in ITZ. The major difference of contour line observed was the slightly higher chloride content due to the presence of ITZ in width of the micrometer scale. It means higher diffusivity in ITZ compared with cement paste accelerated the diffusion of chloride within concrete.

For mesoscopic numerical simulation, distribution of aggregate was recognized as the major influence factor for development of chloride [52]. Chloride content on surface of rebar significantly varied with different arrangement and grading of aggregate. Thus, both mean and maximum distribution of chloride ion in terms of random aggregate models became the major consideration. Figures 16 and 17 summarized average content and maximum versus depth regarding diffusivity of ITZ at 50 years and 100 years, respectively. It was clearly noted that chloride content increased as the diffusivity of ITZ increased. An interesting phenomenon observed was that the influence of compensation was larger in higher chloride content. It attributed to a larger diffusion space released in mixed model including compensation part. From the result of numerical simulation, another point should be noted that within the boundary layer in width of 10 mm from surface of concrete, both mean and maximum chloride content were closed to boundary condition, which was recognized as the lower aggregate volume fraction and smaller particle size in this region.

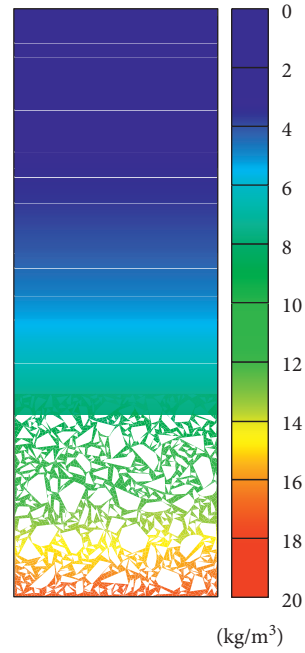

Figure 14: Contour of chloride content of multiscale model.

5.1.2. ITZ Width. The second major factor for chloride diffusion is ITZ width. A thin layer composed of quadrilateral elements in the width of 5 μm, 10 μm, 20 μm, 35 μm, and 50 μm adhering to the edge of aggregates was modeled (Figure 18). For the other parameters, diffusivity of ITZ in $D_{ITZ}/D_{CP} = 5$ was adopted. Maximum particle size of coarse aggregate was limited within $D_{max} = 20$ mm. Figure 18 showed ITZ elements in orange color of FE model in different width of ITZ.

Figures 19 and 20 showed average content and maximum versus depth regarding width of ITZ at 50 years and 100 years, respectively. A clear conclusion was drawn that thicker ITZ width induced higher volume fraction of ITZ and enhanced diffusion of chloride ion.

5.1.3. Aggregate Volume Fraction. Aggregate volume fraction determined total amount of aggregates within given space and accordingly total length of perimeter was also determined, which was the key factor for proportion of ITZ

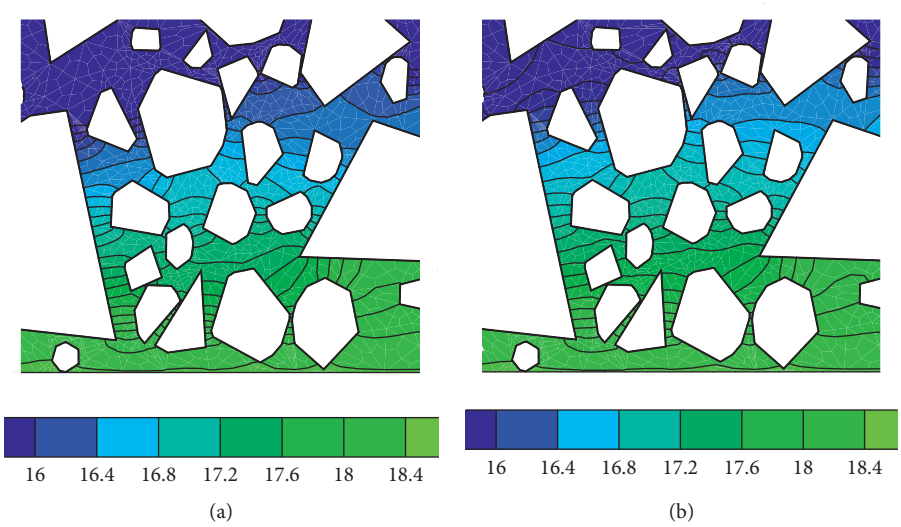

FIGURE 15: Typical distribution of chloride content regarding diffusivity in ITZ (solid line denotes isoline of chloride content). (a) $D_{ITZ}/D_{CP} = 1$. (b) $D_{ITZ}/D_{CP} = 5$.

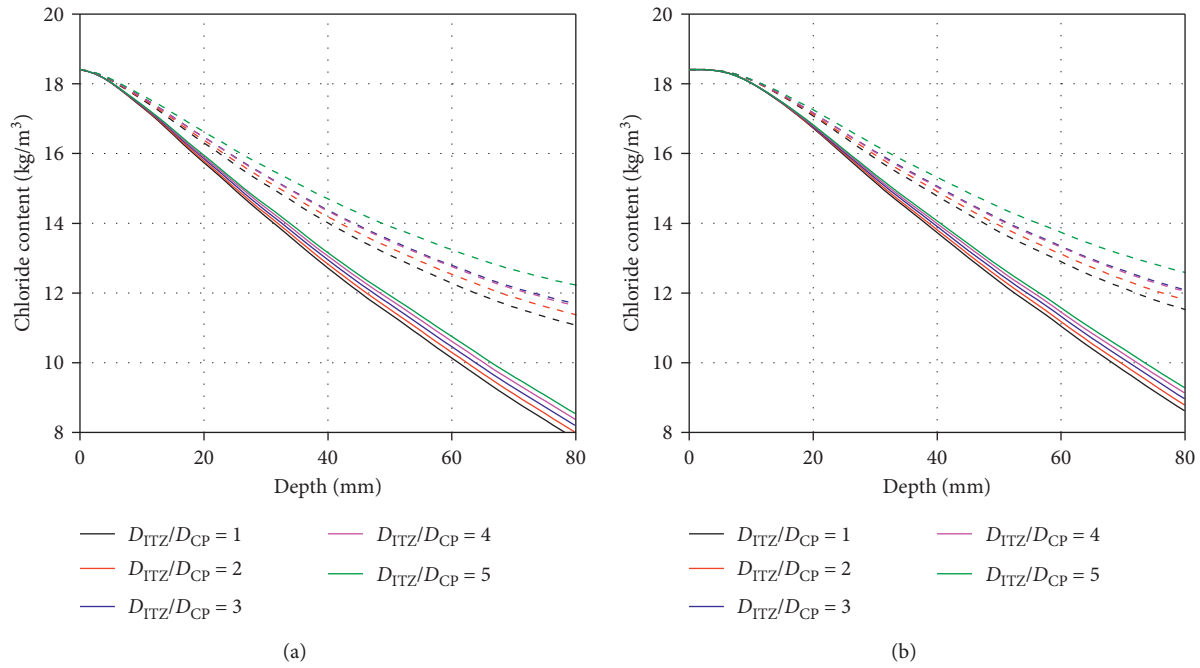

FIGURE 16: Average content and maximum vs. depth regarding compensation and ITZ D_{ITZ}/D_{CP} at 50 y of exposure (dashed: w/o compensation; solid: with compensation). (a) Mean chloride content. (b) Maximum chloride content.

in concrete. In this section, the cases of aggregate volume fraction in 20%, 30%, 40%, 50%, 60%, and 70% were discussed by means of the approach introduced in this paper. Diffusivity of ITZ in $D_{ITZ}/D_{CP} = 5$ and 50 μm of ITZ width were adopted. Maximum aggregate size in 20 mm and Fuller grading was adopted. Both types of cases with compensation and without compensation were studied. Figure 21 showed with aggregate volume fraction from 20% to 70%, the typical distribution of chloride content and aggregate with given analysis square space.

Figure 22 described mean content and maximum versus depth regarding aggregate volume fraction at 100 years. According to the result, presence of ITZ provided greater effect on higher aggregate volume fraction and thus reduced the difference of chloride content profile in cases with different aggregate volume fraction.

5.1.4. Grade of Aggregate. The cases for grade of aggregate with maximum aggregate size $D_{max} = 5$ mm, 10 mm, 15 mm, 20 mm, 25 mm, and 30 mm were discussed. Both cases with or without ITZ were included. Fuller grading was adopted. For the case with ITZ, diffusivity of ITZ in $D_{ITZ}/D_{CP} = 5$ was adopted. 50 μm of ITZ width was modeled by expanding the

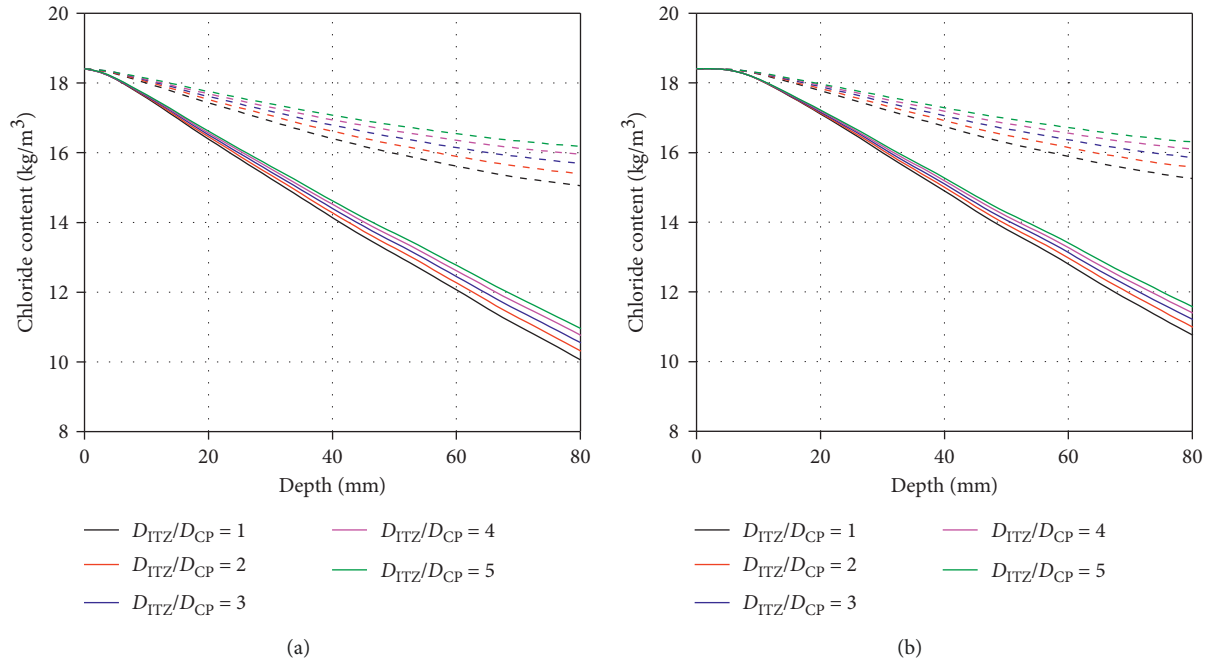

Figure 17: Average content and maximum vs. depth regarding compensation and ITZ D_{ITZ}/D_{CP} at 100 y of exposure (dashed: w/o compensation; solid: with compensation). (a) Mean chloride content. (b) Maximum chloride content.

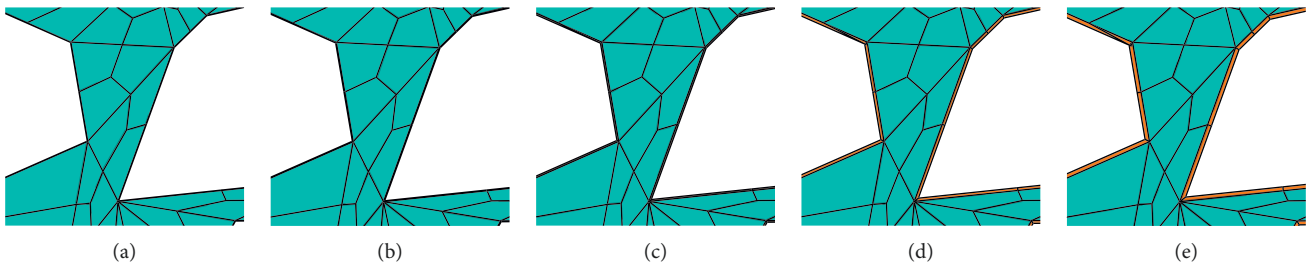

Figure 18: FE model for cement paste and ITZ regarding ITZ width, h (blue: cement paste; orange: ITZ). (a) $h = 5\,\mu$m. (b) $h = 10\,\mu$m. (c) $h = 20\,\mu$m. (d) $h = 35\,\mu$m. (e) $h = 50\,\mu$m.

edge of aggregate and rebar. Both types of cases with compensation and without compensation were studied. Figure 23 showed with maximum aggregate size from 5 mm to 30 mm, the typical distribution of chloride content and aggregate with given analysis square space. Figure 24 showed mean content and maximum versus depth regarding grade of aggregate at 100 years.

Figure 24 summarized mean and maximum chloride content vs. depth from surface of concrete. An interesting point should be noted that the lower aggregate volume fraction and smaller particle size in the region closed to boundary was not significant in the case with smaller maximum particle size. Moreover, presence of ITZ indeed enhanced diffusion of chloride ion especially in cases with smaller maximum particle size.

5.2. Chloride Content and Corrosion of Steel Rebar. In this section, chloride content on the front of rebar in terms of the configuration was studied by the multiscale numerical simulation introduced previously. According to general engineering design, a group of concrete cover thickness and rebar diameter was devised for detailed comparison of chloride diffusion and rebar corrosion, shown in Table 1. For the purpose of comparison, rebar in diameter of 16 mm was selected for the cases in different cover thickness and 50 mm cover thickness for the comparison of rebar diameters. By means of the random aggregate generation approach and considering reasonable computing loading, 100 two-dimensional samples for each combination of concrete cover thickness and rebar diameter was modeled considering random distribution of aggregate.

Considering three-phase composite of concrete, nodes and elements of ITZ were modeled not only surrounding aggregate, but also on the surface of steel rebar. It also justified to a certain extent that the formation of ITZ on surface of steel rebar in the light of the same mechanism of aggregate. Therefore the same width and diffusivity of ITZ on surface of steel were adopted. Chloride content on front of rebar was extracted from the newly created nodes on the edge of ITZ elements in terms of the neat surface of steel rebar.

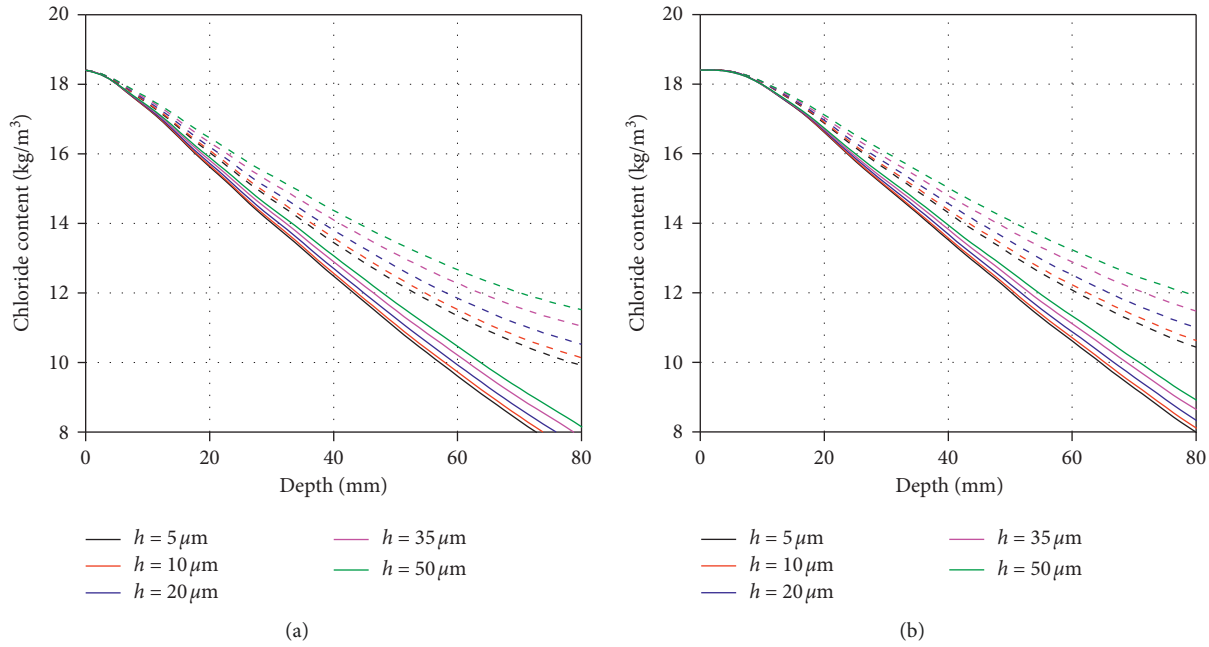

Figure 19: Average content and maximum vs. depth regarding compensation and ITZ width at 50 y of exposure (dashed: w/o compensation; solid: with compensation). (a) Mean chloride content. (b) Maximum chloride content.

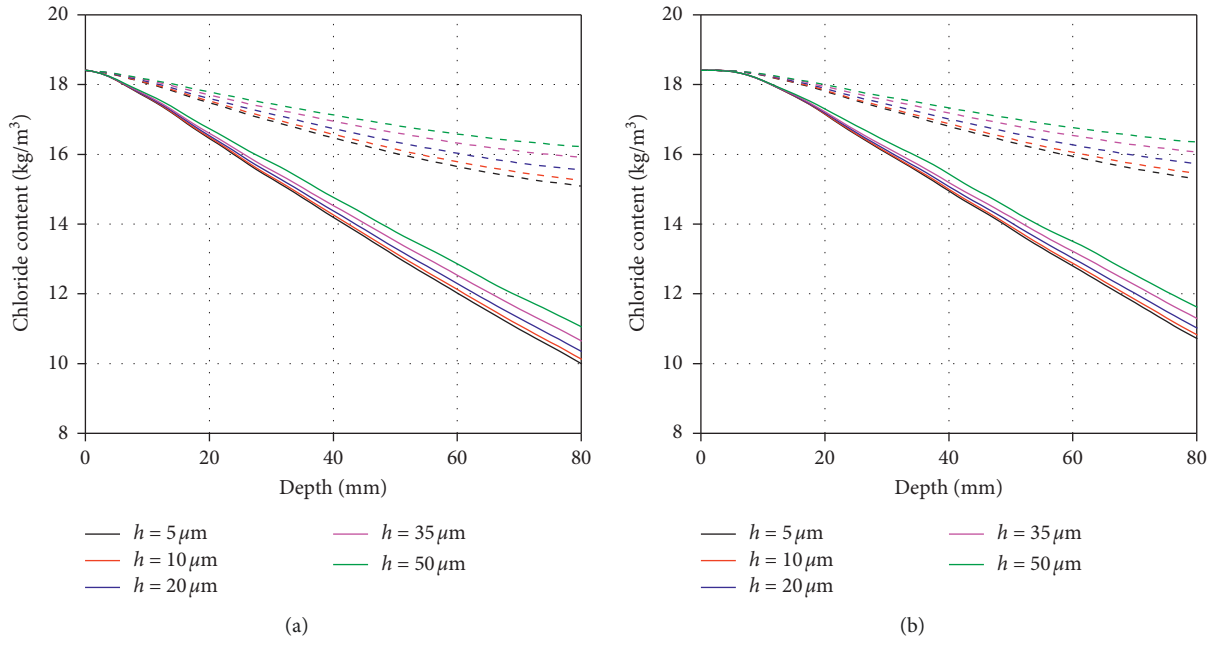

Figure 20: Average content and maximum vs. depth regarding compensation and ITZ width at 100 y of exposure (dashed: w/o compensation; solid: with compensation). (a) Mean chloride content. (b) Maximum chloride content.

The placement of steel rebar on the center of straight edge was considered. Rebar placed in the center of bottom side of concrete section (Figure 25(a) listed in Table 1 was tested. Term d denotes the cover thickness and the diameter; D of circle refers to diameter of rebar. A two-dimensional mesoscopic core model in the size of 100×100 mm was created. In order to guarantee the effect of compensation, 100×200 mm total size of compensation model was designed as two times of core model. 10 mm thickness of ITL was considered for compensation process. Apart from ITZ elements surrounding aggregates, new elements adjacent to steel rebar were also modeled by expanding outline. Therefore, chloride content on surface of rebar was extracted from the newly built nodes of ITZ. Both types of cases with compensation and without compensation were studied. Diffusivity of ITZ in D_{ITZ}/

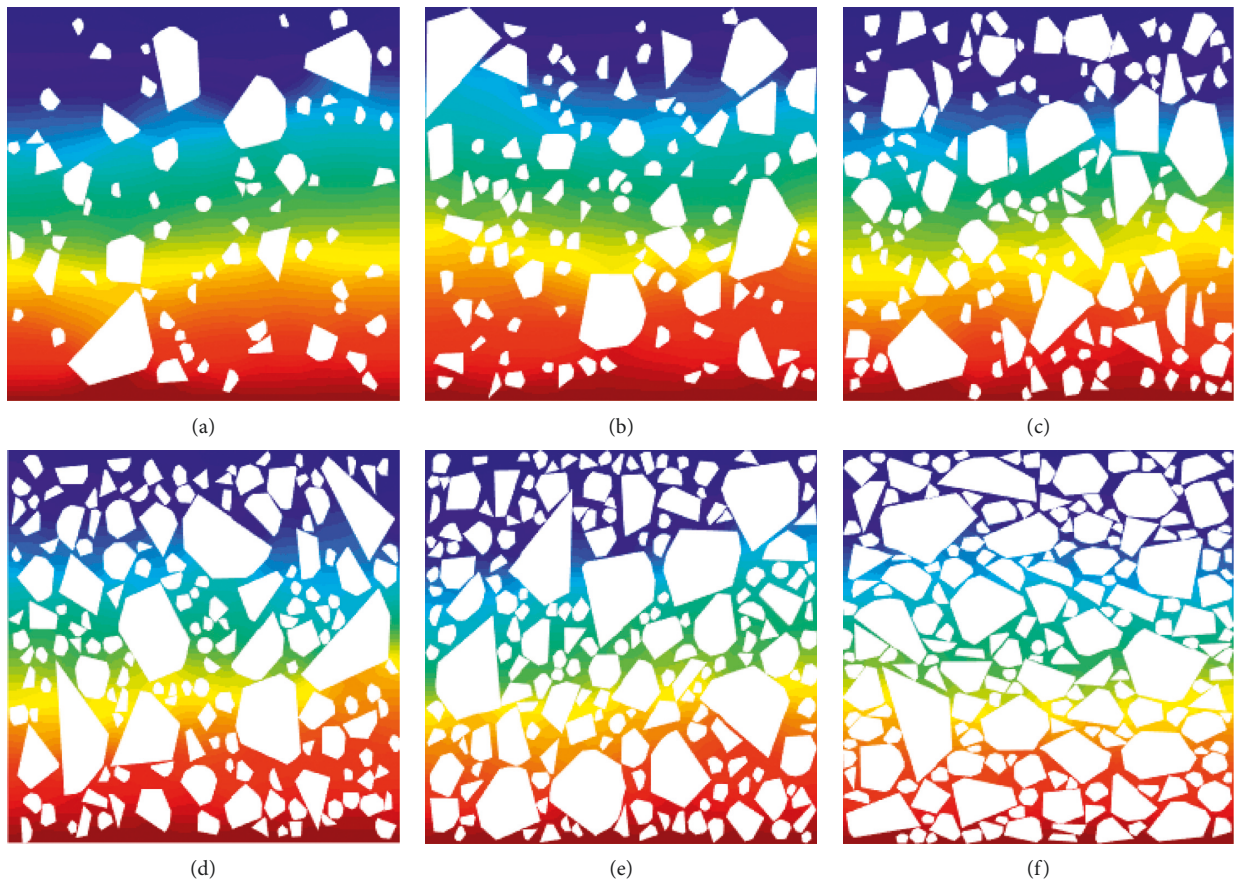

Figure 21: FE model and typical distribution of chloride content for different aggregate volume fraction, fa. (a) fa = 20%. (b) fa = 30%. (c) fa = 40%. (d) fa = 50%. (e) fa = 60%. (f) fa = 70%.

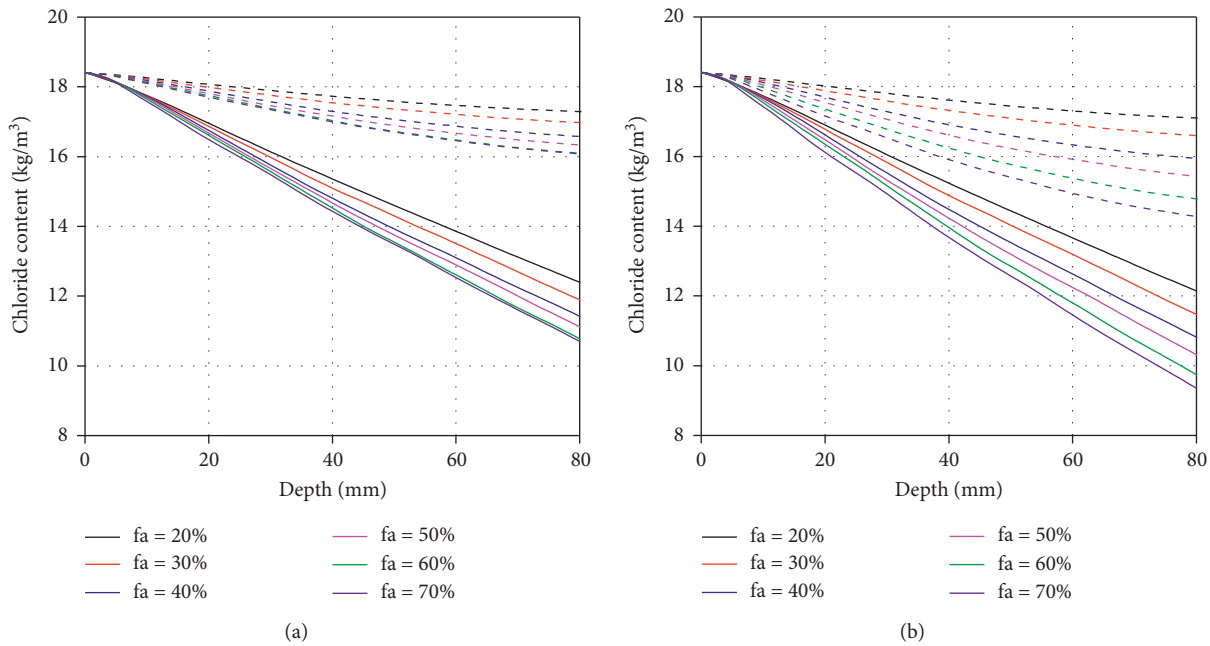

Figure 22: Continued.

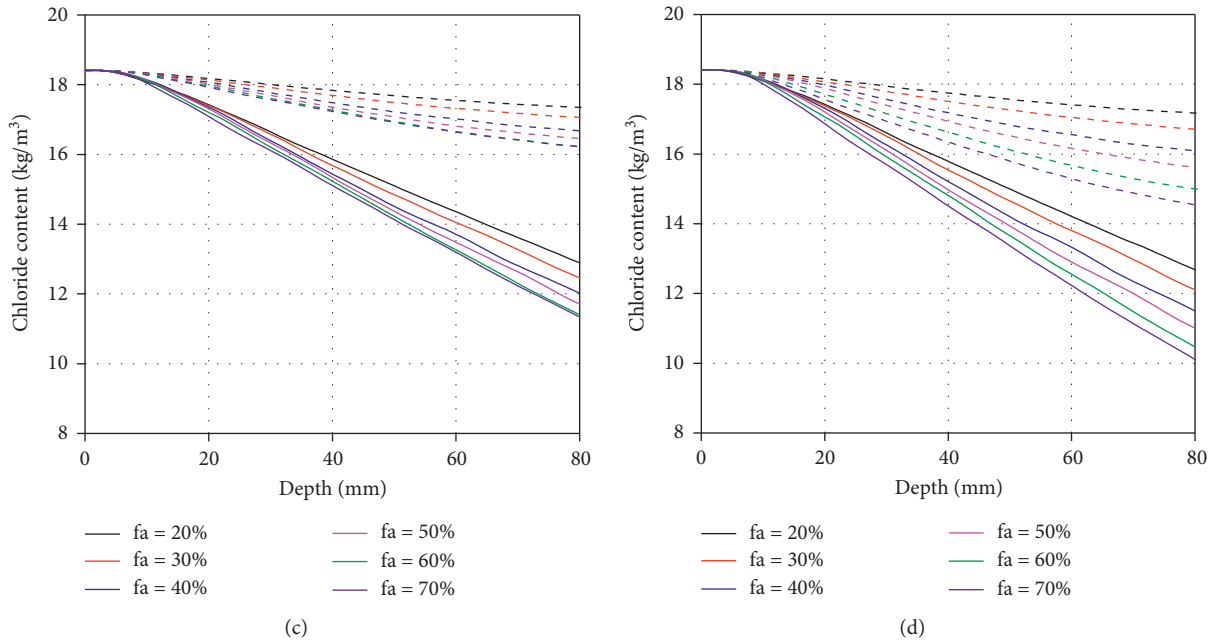

FIGURE 22: Average content and maximum vs. depth regarding aggregate volume fraction (fa) and presence of ITZ at 100 y of exposure (dashed: w/o compensation; solid: with compensation). (a) Mean chloride content with ITZ. (b) Mean chloride content w/o ITZ. (c) Max chloride content with ITZ. (d) Max chloride content w/o ITZ.

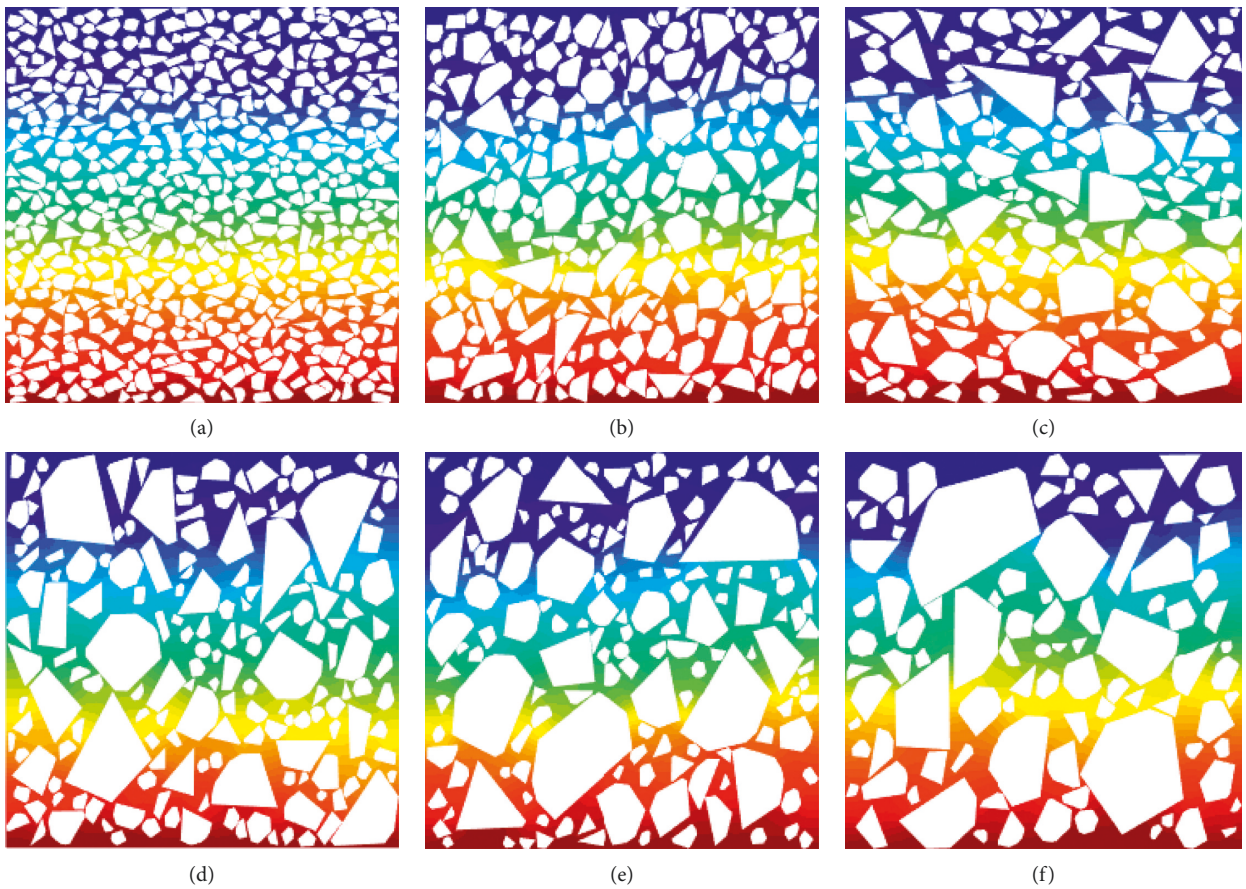

FIGURE 23: FE model and typical distribution of chloride content for different aggregate and gradation. (a) $D_{max} = 5$ mm. (b) $D_{max} = 10$ mm. (c) $D_{max} = 15$ mm. (d) $D_{max} = 20$ mm. (e) $D_{max} = 25$ mm. (f) $D_{max} = 30$ mm.

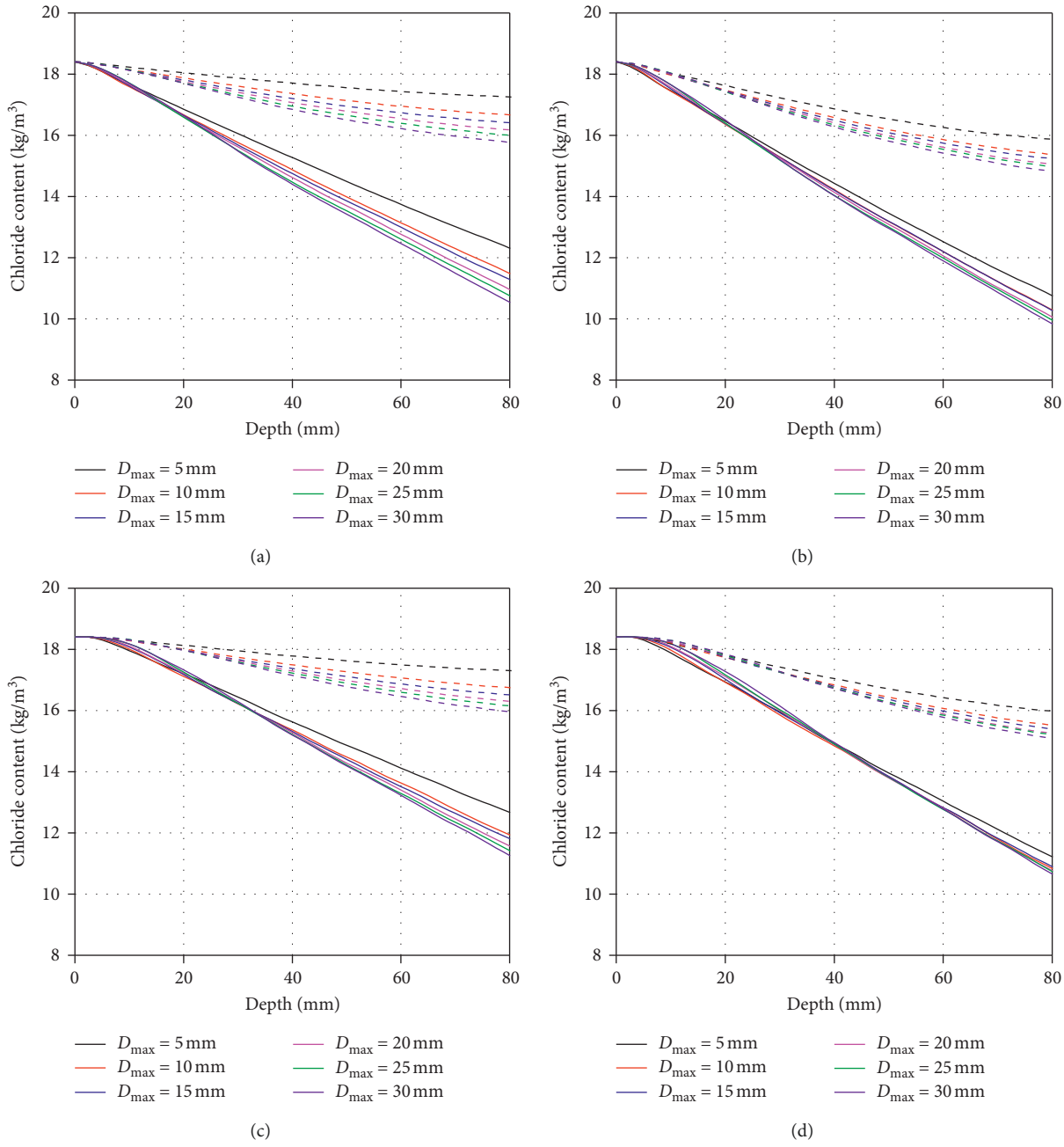

Figure 24: Average content and maximum vs. depth, regarding grade of aggregate and presence of ITZ (dashed: w/o compensation; solid: with compensation). (a) Mean with ITZ. (b) Mean w/o ITZ. (c) Max with ITZ. (d) Max w/o ITZ.

Table 1: Details of model comparison for concrete cover thickness and rebar diameter regarding chloride diffusion and rebar corrosion.

Cover thickness, C (mm)	Rebar diameter, D (mm)				
	12	16	20	25	28
20		×			
30		×			
40		×			
50	×	×	×	×	×
60		×			

$D_{CP} = 5$ was adopted. 50 μm of ITZ width was modeled by expanding the edge of aggregate and rebar. Maximum aggregate size in 20 mm was considered, and Fuller grading was adopted.

Figure 25(b) showed typical distribution of chloride content within core mesoscopic model and compensated macroscopic model at 100 years of exposure period for the cases of rebar placed in center of bottom. The contour clearly described sound transition of chloride content near ITL on both cases and proved the effect of compensation as well.

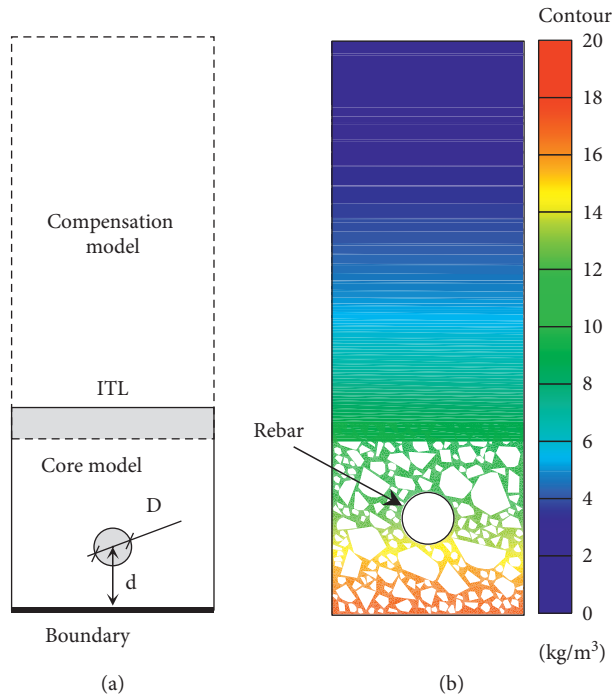

Figure 25: Geometrical configuration and chloride content distribution of compensation case. (a) Geometrical configuration of concrete analysis space and rebar. (b) Typical distribution of aggregate and chloride content in concrete, 100 y.

The circle curve of rebar was meshed into a series of node, and nodal chloride content was obtained from result of FE analysis. For all 100 samples of each research case, mean value of chloride content on each node around rebar was calculated and plotted in polar coordinate. Figure 26 showed the polar distribution of mean chloride content on cross section of rebar at 20 years (solid) and 100 years (dashed) of exposure period. Depending on whether compensation model or ITZ was considered, chloride content was plotted in different colors, shown in legend on the bottom. Distribution of chloride content developed towards lower-middle, which matched the configuration of boundary condition. Result indicated higher chloride content was obtained for longer period of exposure. Moreover, lower value was observed in the cases with compensation.

Mean chloride content vs. cover thickness for 16 mm rebar and mean chloride content vs. diameter for 50 mm cover are summarized in Figure 27. An obvious result showed lower chloride content in compensation case since solid lines were all under corresponding dashed lines in the figures, which attributed the larger diffusion space in compensation cases.

Another observation was the insignificant difference between the solid line of "ITZ" and "ITZ + Compensation" (20 years). Since diffusion of chloride did not exceed the border of core part and compensation part, there was no clear difference for both diffusion spaces of "ITZ" and "ITZ + Compensation," which is the major reason.

The corrosion model regressed by Liu and Weyers [34] based on experimental data included the influence of chloride content, temperature, concrete cover resistance, and time of cement hydration, which was expressed as

$$\ln\left(1.08 i_{\text{corr}}\right) = 8.37 + 0.618 \cdot \ln\left(1.69\text{Cl}\right) - \frac{3034}{T} - 0.000105 R_{\text{c}} + 2.32 t^{-0.215}, \tag{21}$$

where i_{corr} is corrosion current intensity (μA/cm^2); Cl is chloride content (kg/m^3), which was obtained from numerical simulation result of chloride diffusion; T is temperature at the depth of steel surface (in degree Kelvin); R_{c} is the resistance of the cover concrete (ohms); and t is corrosion time duration (years). For corrosion calculation in the following discussion, environmental temperature 293 K was adopted. A generally adopted value of concrete resistance 1500 Ω was adopted. Besides, pitting of rebar was neglected. With the data chloride content obtained by numerical simulation, the real-time corrosion current rate at each time step of numerical simulation was calculated. The corrosion depth on surface of rebar was calculated as [50]

$$D_{t+\Delta t} = D_t - 0.023 \cdot i_{\text{corr}} \Delta t, \tag{22}$$

where D_t is remaining rebar diameter (mm) at t years, here 20 mm adopted and $D_{t+\Delta t}$ is reduced rebar diameter (mm) at $t + \Delta t$ years.

A single mean chloride content for each time step was calculated as the attacking chloride content for rebar, and mean corrosion depth of rebar was calculated based on equation (19). Figure 28(a) (cover thickness) and Figure 28(b) (rebar diameter) showed corrosion process and

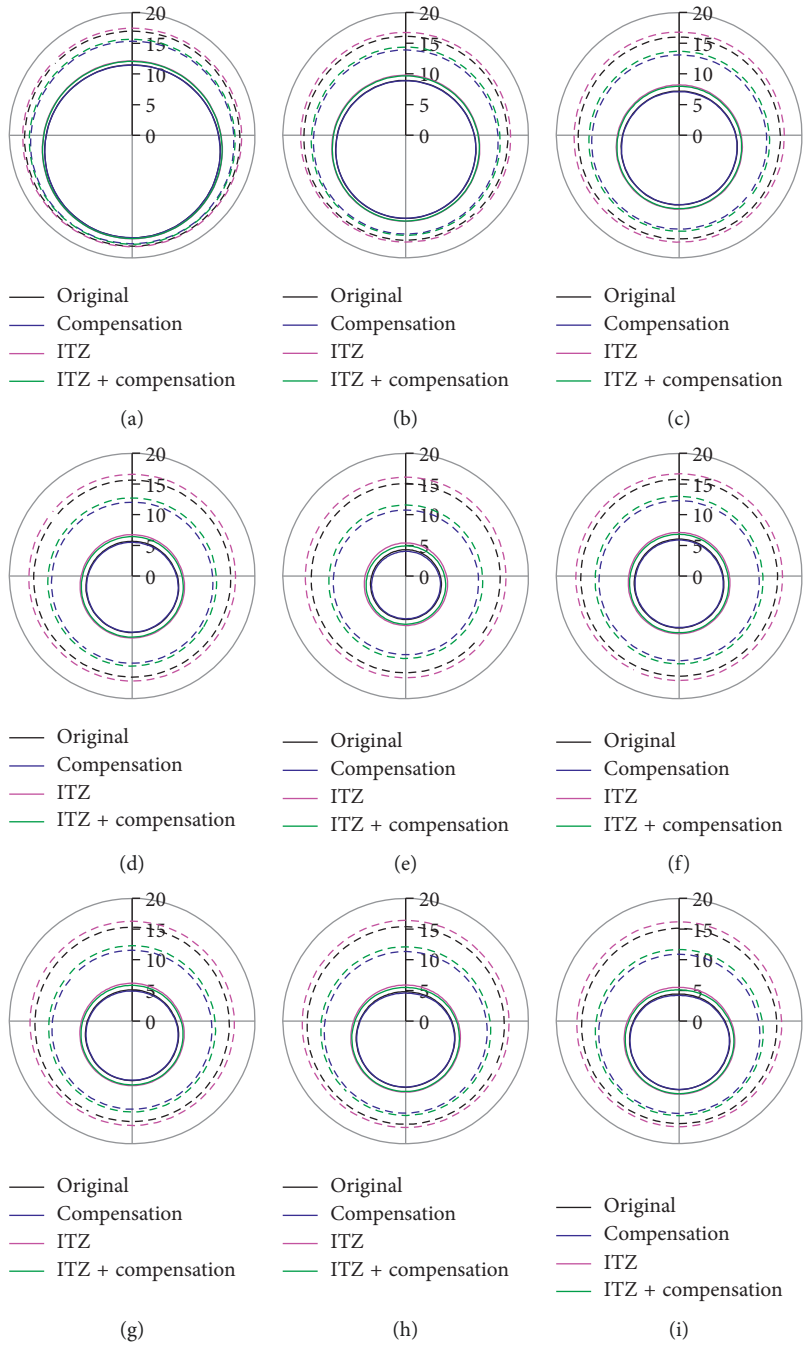

Figure 26: Polar distribution of chloride content on cross section of rebar on center of bottom side (solid: 20 y; dashed: 100 y). (a) $R = 16$ mm, $C = 20$ mm. (b) $R = 16$ mm, $C = 30$ mm. (c) $R = 16$ mm, $C = 40$ mm. (d) $R = 16$ mm, $C = 50$ mm. (e) $R = 16$ mm, $C = 60$ mm. (f) $R = 12$ mm, $C = 50$ mm. (g) $R = 20$ mm, $C = 50$ mm. (h) $R = 25$ mm, $C = 50$ mm. (i) $R = 28$ mm, $C = 50$ mm.

characteristics of rebar based on obtained distribution of chloride content around rebar. Ordinate in these figures indicated the ratio of diameter of corroded rebar to initial value.

Obtained diagrams showed less corrosion of steel rebar in the cases with compensation due to larger space for chloride diffusion and lower distributed chloride content. More obvious difference comparing between the result from the compensation model (solid) and the case without compensation (dashed) due to a longer exposure period was observed.

Moreover, it should be noted that increasing concrete cover provided slight effect on protecting steel rebar from corrosion. The higher diffusivity in ITZ adhering on steel rebar provided an equivalent express channel for diffusion of chloride ion around steel rebar. Thus, ITZ actually balanced the difference of depth from surface of concrete for these cases and insignificant difference was observed for cases in different covers. Similar phenomenon was noticed that compensation decreased chloride content on surface of rebar as well as its corrosion degree.

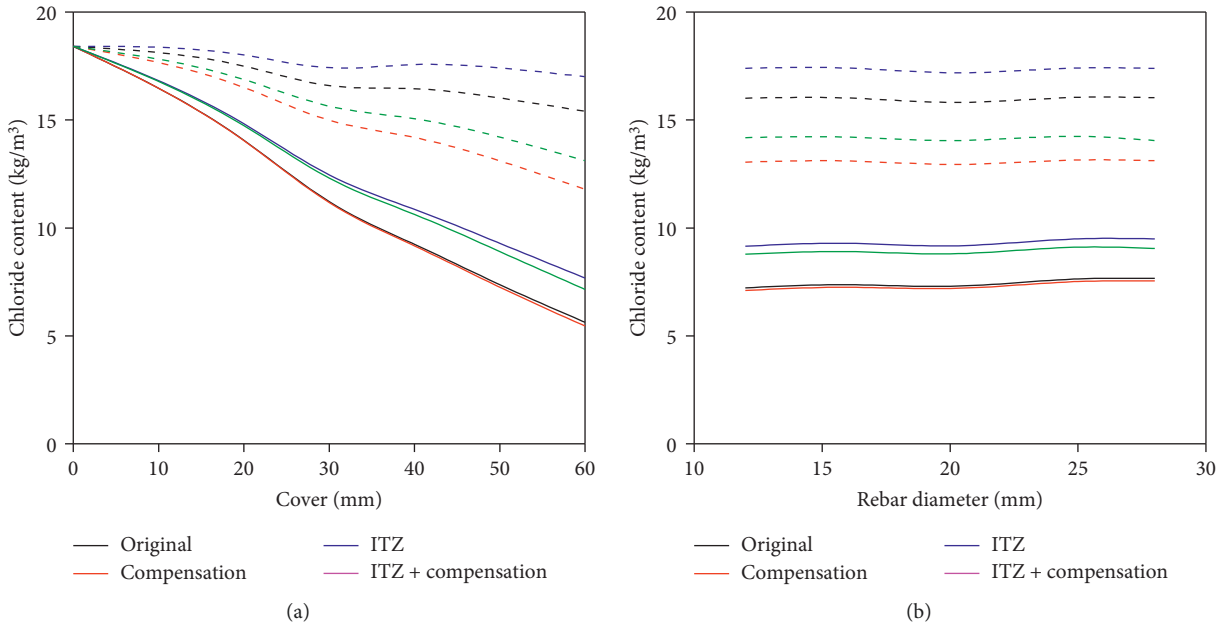

Figure 27: Mean chloride content of rebar on center of bottom side (solid: 20 y; dashed: 100 y). (a) Mean chloride content vs. cover thickness, 16 mm rebar. (b) Mean chloride content vs. diameter, 50 mm cover.

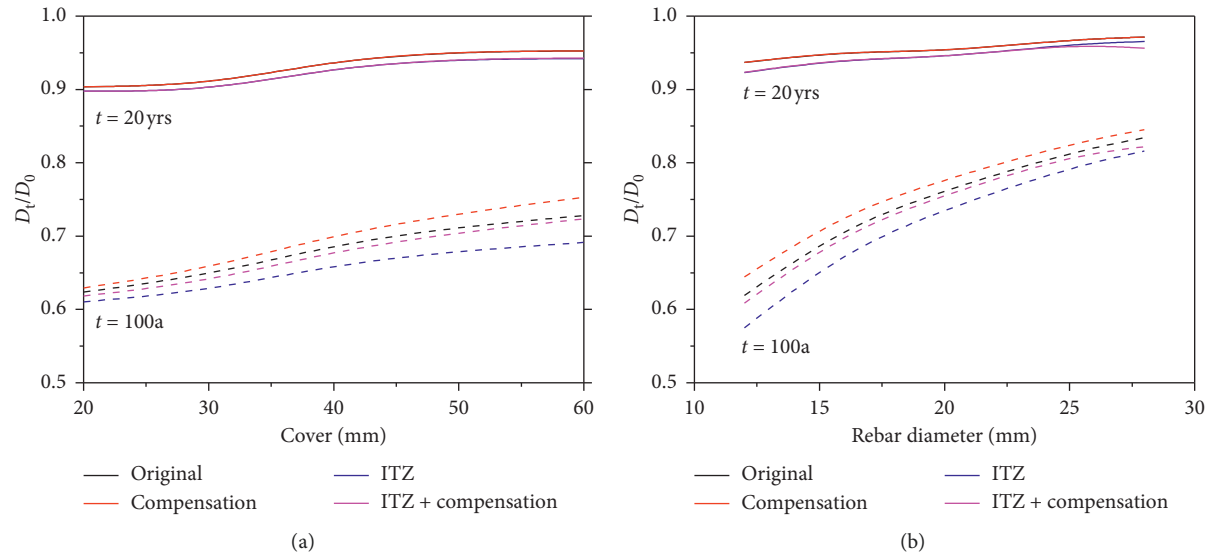

Figure 28: Mean chloride content of rebar on center of bottom side (solid: 20 y; dashed: 100 y). (a) Mean remaining diameter vs. cover thickness, 16 mm rebar. (b) Mean remaining diameter vs. diameter, 50 mm cover.

6. Conclusion

This paper presented a study on the approach of multiscale modeling for diffusion of chloride ion within concrete including ITZ. A two-phase integrated model including core part and compensation part was introduced, where both phases were connected by an overlapped zone called interfacial transition layer. Nodes and elements of ITZ in FE model were built by expanding outline of aggregates which were randomly generated. Cases considering multiscale and ITZ were studied for obtaining chloride content profile. Moreover, corrosion of rebar on straight edge was discussed by means of the multiscale approach. The conclusions of this study are summarized as follows:

(1) The multiscale approach based on the theory of compensation for mesoscopic numerical simulation of chloride diffusion within concrete introduced in this paper was applied by means of numerical simulation. The presented work showed the influence of compensated model on distribution of chloride content, which provided the basis for future large-scale structural durability analysis in optimized size, number of DOFs, and time consumption.

(2) Regarding diffusivity and width of ITZ, volume fraction, and grade of aggregate, effects of ITZ on distribution of chloride were compared in the presented work. The result showed significant difference on distribution of chloride content between different configuration of ITZ and compensation.

(3) In the light of corrosion model of steel rebar in terms of surrounding chloride content, presence of ITZ and multiscale compensation was discussed by numerical simulation. The result obtained is related to the configuration of rebar diameter, concrete cover, and exposure period. It was clearly concluded that consideration of both ITZ and compensation changed significantly the distribution of chloride content as well as corrosion process of steel rebar.

Data Availability

The data used to support the findings of this study are available from the corresponding author upon request.

Conflicts of Interest

The authors declare that they have no conflicts of interest.

Acknowledgments

This study was sponsored by the National Key Research and Development Program of China (2016YFC0701202). This study was also supported by the National Natural Science Foundation of China (51508053), the National Natural Science Foundation of China (51808069), and the Fundamental Research Funds for the Central Universities (106112014CDJZR200016), which were greatly appreciated by the authors.

References

[1] W. Zhu, R. François, Q. Fang, and D. Zhang, "Influence of long-term chloride diffusion in concrete and the resulting corrosion of reinforcement on the serviceability of RC beams," *Cement and Concrete Composites*, vol. 71, pp. 144–152, 2016.

[2] Q.-F. Liu, G.-L. Feng, J. Xia, J. Yang, and L.-Y. Li, "Ionic transport features in concrete composites containing various shaped aggregates: a numerical study," *Composite Structures*, vol. 183, pp. 371–380, 2018.

[3] U. Angst, B. Elsener, C. K. Larsen, and Ø. Vennesland, "Critical chloride content in reinforced concrete–a review," *Cement and Concrete Research*, vol. 39, no. 12, pp. 1122–1138, 2009.

[4] J.-J. Zheng, H. S. Wong, and N. R. Buenfeld, "Assessing the influence of ITZ on the steady-state chloride diffusivity of concrete using a numerical model," *Cement and Concrete Research*, vol. 39, no. 9, pp. 805–813, 2009.

[5] L.-X. Mao, Z. Hu, J. Xia et al., "Multi-phase modelling of electrochemical rehabilitation for ASR and chloride affected concrete composites," *Composite Structures*, vol. 207, pp. 176–189, 2019.

[6] J. Xu and F. Li, "A meso-scale model for analyzing the chloride diffusion of concrete subjected to external stress," *Construction and Building Materials*, vol. 130, pp. 11–21, 2017.

[7] X. Du, L. Jin, and G. Ma, "A meso-scale numerical method for the simulation of chloride diffusivity in concrete," *Finite Elements in Analysis and Design*, vol. 85, pp. 87–100, 2014c.

[8] F. Bernard and S. Kamali-Bernard, "Numerical study of ITZ contribution on mechanical behavior and diffusivity of mortars," *Computational Materials Science*, vol. 102, pp. 250–257, 2015.

[9] J.-J. Zheng and X.-Z. Zhou, "Effective medium method for predicting the chloride diffusivity in concrete with ITZ percolation effect," *Construction and Building Materials*, vol. 47, pp. 1093–1098, 2013.

[10] K. Wu, L. Xu, G. D. Schutter, H. Shi, and G. Ye, "Influence of the interfacial transition zone and interconnection on chloride migration of portland cement mortar," *Journal of Advanced Concrete Technology*, vol. 13, no. 3, pp. 169–177, 2015.

[11] Z. Zhang and Q. Zhang, "Self-healing ability of engineered cementitious composites (ECC) under different exposure environments," *Construction and Building Materials*, vol. 156, pp. 142–151, 2017.

[12] Z. Zhang and Q. Zhang, "Matrix tailoring of engineered cementitious composites (ECC) with non-oil-coated, low tensile strength PVA fiber," *Construction and Building Materials*, vol. 161, pp. 420–431, 2018.

[13] H. Chen, Z. Zhu, J. Lin, W. Xu, and L. Liu, "Numerical modeling on the influence of particle shape on ITZ's microstructure and macro-properties of cementitious composites: a critical review," *Journal of Sustainable Cement-Based Materials*, vol. 7, no. 4, pp. 248–269, 2018.

[14] J. F. Unger and S. Eckardt, "Multiscale modeling of concrete," *Archives of Computational Methods in Engineering*, vol. 18, no. 3, pp. 341–393, 2011.

[15] G.-L. Feng, L.-Y. Li, B. Kim, and Q.-F. Liu, "Multiphase modelling of ionic transport in cementitious materials with surface charges," *Computational Materials Science*, vol. 111, pp. 339–349, 2016.

[16] K. Maekawa, T. Ishida, and T. Kishi, "Multi-scale modeling of concrete performance," *Journal of Advanced Concrete Technology*, vol. 1, no. 2, pp. 91–126, 2003.

[17] L. Chen, Z. Qian, and J. Wang, "Multiscale numerical modeling of steel bridge deck pavements considering vehicle–pavement interaction," *International Journal of Geomechanics*, vol. 16, no. 1, article B4015002, 2016.

[18] Y. Hiratsuka and K. Maekawa, "Multi-scale and multi-chemo-physics analysis applied to fatigue life assessment of strengthened bridge decks," in *Proceedings of XIII International Conference on Computational Plasticity: fundamentals and applications*, pp. 596–607, Barcelona, Spain, September 2015.

[19] X. Tu et al., "A multiscale numerical simulation approach for chloride diffusion and rebar corrosion with compensation model," *Computers and Concrete*, vol. 21, no. 4, pp. 471–484, 2018.

[20] X. Wang, M. Zhang, and A. P. Jivkov, "Computational technology for analysis of 3D meso-structure effects on damage and failure of concrete," *International Journal of Solids and Structures*, vol. 80, pp. 310–333, 2016.

[21] Z. M. Wang, A. K. H. Kwan, and H. C. Chan, "Mesoscopic study of concrete I: generation of random aggregate structure and finite element mesh," *Computers and Structures*, vol. 70, no. 5, pp. 533–544, 1999.

[22] M. Bailakanavar, Y. Liu, J. Fish, and Y. Zheng, "Automated modeling of random inclusion composites," *Engineering with Computers*, vol. 30, no. 4, pp. 609–625, 2012.

[23] Z. Y. Ren and J. Y. W., "Generation of spatial convex polyhedron random aggregate model," in *Proceedings of ICOME 2006*, Hefei, China, October 2006.

[24] A. Caballero, C. M. López, and I. Carol, "3D meso-structural analysis of concrete specimens under uniaxial tension," *Computer Methods in Applied Mechanics and Engineering*, vol. 195, no. 52, pp. 7182–7195, 2006.

[25] F. Biondini, F. Bontempi, D. M. Frangopol, and P. G. Malerba, "Cellular automata approach to durability analysis of concrete structures in aggressive environments," *Journal of Structural Engineering*, vol. 130, no. 11, pp. 1724–1737, 2004.

[26] B. Šavija, J. Pacheco, and E. Schlangen, "Lattice modeling of chloride diffusion in sound and cracked concrete," *Cement and Concrete Composites*, vol. 42, pp. 30–40, 2013.

[27] H. Ma, W. Xu, and Y. Li, "Random aggregate model for mesoscopic structures and mechanical analysis of fully-graded concrete," *Computers and Structures*, vol. 177, pp. 103–113, 2016.

[28] R. François and G. Arliguie, "Effect of microcracking and cracking on the development of corrosion in reinforced concrete members," *Magazine of Concrete Research*, vol. 51, no. 2, pp. 143–150, 1999.

[29] T. Vidal, A. Castel, and R. François, "Corrosion process and structural performance of a 17 year old reinforced concrete beam stored in chloride environment," *Cement and Concrete Research*, vol. 37, no. 11, pp. 1551–1561, 2007.

[30] T. Vidal, A. Castel, and R. François, "Analyzing crack width to predict corrosion in reinforced concrete," *Cement and Concrete Research*, vol. 34, no. 1, pp. 165–174, 2004.

[31] R. Zhang, A. Castel, and R. François, "Concrete cover cracking with reinforcement corrosion of RC beam during chloride-induced corrosion process," *Cement and Concrete Research*, vol. 40, no. 3, pp. 415–425, 2010.

[32] R. Zhang, A. Castel, and R. François, "The corrosion pattern of reinforcement and its influence on serviceability of reinforced concrete members in chloride environment," *Cement and Concrete Research*, vol. 39, no. 11, pp. 1077–1086, 2009.

[33] C. Andrade, C. Alonso, and F. J. Molina, "Cover cracking as a function of bar corrosion: Part I-Experimental test," *Materials and Structures*, vol. 26, no. 8, pp. 453–464, 1993.

[34] T. Liu and R. W. Weyers, "Modeling the dynamic corrosion process in chloride contaminated concrete structures," *Cement and Concrete Research*, vol. 28, no. 3, pp. 365–379, 1998.

[35] L. C. Qing, "Corrosion initiation of reinforcing steel in concrete under natural salt spray and service loading—results and analysis," *Materials Journal*, vol. 97, no. 6, 2000.

[36] S. M. Pritpal and S. E. Mahmoud, "Flexural strength of concrete beams with corroding reinforcement," *ACI Structural Journal*, vol. 96, no. 1, 1999.

[37] A. A. Torres-Acosta, S. Navarro-Gutierrez, and J. Terán-Guillén, "Residual flexure capacity of corroded reinforced concrete beams," *Engineering Structures*, vol. 29, no. 6, pp. 1145–1152, 2007.

[38] A. A. Torres-Acosta and M. Martnez-Madrid, "Residual life of corroding reinforced concrete structures in marine environment," *Journal of Materials in Civil Engineering*, vol. 15, no. 4, pp. 344–353, 2003.

[39] F. Biondini, F. Bontempi, D. M. Frangopol, and P. G. Malerba, "Probabilistic service life assessment and maintenance planning of concrete structures," *Journal of Structural Engineering*, vol. 132, no. 5, pp. 810–825, 2006.

[40] P. Zhang, D. Li, Y. Qiao, S. Zhang, C. Sun, and T. Zhao, "Effect of air entrainment on the mechanical properties, chloride migration, and microstructure of ordinary concrete and fly ash concrete," *Journal of Materials in Civil Engineering*, vol. 30, no. 10, article 04018265, 2018.

[41] P. Zhang, F. H. Wittmann, M. Vogel, H. S. Müller, and T. Zhao, "Influence of freeze-thaw cycles on capillary absorption and chloride penetration into concrete," *Cement and Concrete Research*, vol. 100, pp. 60–67, 2017.

[42] P. Zhang, D. Hou, Q. Liu, Z. Liu, and J. Yu, "Water and chloride ions migration in porous cementitious materials: an experimental and molecular dynamics investigation," *Cement and Concrete Research*, vol. 102, pp. 161–174, 2017.

[43] X. Li, F. Wu, and Z. Huang, "Analytical solution to chloride diffusion equation on concrete," *Concrete(Chinese)*, vol. 30, no. 10, pp. 30–33, 2009.

[44] W. Dridi, "Analysis of effective diffusivity of cement based materials by multi-scale modelling," *Materials and Structures*, vol. 46, no. 1-2, pp. 313–326, 2012.

[45] G. Sun, Y. Zhang, W. Sun, Z. Liu, and C. Wang, "Multi-scale prediction of the effective chloride diffusion coefficient of concrete," *Construction and Building Materials*, vol. 25, no. 10, pp. 3820–3831, 2011.

[46] Z. Zhu, H. Chen, L. Liu, and X. Li, "Multi-scale modelling for diffusivity based on practical estimation of interfacial properties in cementitious materials," *Powder Technology*, vol. 307, pp. 109–118, 2017.

[47] K. Maekawa, T. Ishida, and T. Kishi, *Multi Scale Modeling of Structural Concrete*, Taylor & Francis, Vol. 670, Taylor & Francis, Abingdon, UK, 2009.

[48] Q. Yuan, C. Shi, G. De Schutter, K. Audenaert, and D. Deng, "Chloride binding of cement-based materials subjected to external chloride environment: a review," *Construction and Building Materials*, vol. 23, no. 1, pp. 1–13, 2009.

[49] P. S. Mangat and B. T. Molloy, "Prediction of long term chloride concentration in concrete," *Materials and Structures*, vol. 27, no. 6, pp. 338–346, 1994.

[50] B. Šavija, M. Luković, J. Pacheco, and E. Schlangen, "Cracking of the concrete cover due to reinforcement corrosion: a two-dimensional lattice model study," *Construction and Building Materials*, vol. 44, pp. 626–638, 2013.

[51] Y. Zhao et al., "Concrete surface chloride ion concentration varying with seasons in marine environment (Chinese)," *Journal of Zhejiang University (Engineering Science)*, vol. 43, no. 11, pp. 2120–2124, 2009.

[52] Z. Pan, A. Chen, and X. Ruan, "Spatial variability of chloride and its influence on thickness of concrete cover: a two-dimensional mesoscopic numerical research," *Engineering Structures*, vol. 95, pp. 154–169, 2015.